POWER SYSTEM STABILIZER DESIGN USING OUT OF PHASE TORQUE CORRECTION METHOD

By

Akram Amir Mustafa Saad

Abdelrahman A. Karrar
Professor of Electrical Engineering
(Committee Chair)

Ahmed H. Eltom
Professor of Electrical Engineering
(Committee Member)

Gary L. Kobet
Adjunct Professor of Electrical Engineering
(Committee Member)

POWER SYSTEM STABILIZER DESIGN USING OUT OF PHASE TORQUE CORRECTION METHOD

By

Akram Amir Mustafa Saad

A Thesis Submitted to the Faculty of the University of
Tennessee at Chattanooga in Partial
Fulfillment of the Requirements of the Degree
of Master of Science: Engineering

The University of Tennessee at Chattanooga
Chattanooga, Tennessee

August 2018

ABSTRACT

The need for power system stabilizers (PSS) in interconnected power systems has become essential to damp low frequency oscillations and enhance the system stability. Conventional PSS design techniques utilize local measurements, hence allowing the use of single machine infinite bus method to tune the PSS parameters. However, these techniques do not provide a direct method to calculate the PSS gain.

In this work, an explicit expression based on frequency analysis was derived that relates the PSS function and generator electrical torques. It showed that the torques developed at poorly damped modes have large imaginary component that do not contribute to damping. The PSS is tuned to correct the phase of these torques, thus, provide positive damping.

The proposed method was examined on several test systems namely two-area four-machine, IEEE9, and IEEE39-bus system. Besides successfully improving the system damping, the proposed method was found to be robust at different loading conditions.

TABLE OF CONTENTS

ABSTRACT iii

LIST OF TABLES vi

LIST OF FIGURES vii

CHAPTER

1. INTRODUCTION 1

1.1 BACKGROUND 1
1.2 PROBLEM STATEMENT 1
1.3 OBJECTIVE 2
1.4 STUDY OUTLINE 2

2. LITERATURE REVIEW 3

2.1 INTRODUCTION 3
2.2 ROTOR ANGLE STABILITY 3
2.3 HEFFRON AND PHILLIPS MODEL OF SINGLE MACHINE-INFINITE BUS SYSTEM 5
2.3.1 The effect of excitation system on damping torque 8
2.3.2 The role of the power system stabilizer 9
2.4 POWER SYSTEM STABILIZER DESIGNING APPROACHES 10
2.5 POWER SYSTEM STABILIZER TUNING CONCEPTS 15

3. METHODOLOGY 17

3.1 BACKGROUND 18
3.1.1 State space models 18
3.1.2 Equilibrium points and linearization 18
3.1.3 Eigenvalues 21
3.2 GENERATOR ELECTRICAL TORQUES 21
3.3 SINGLE MACHINE INFINITE BUS SYSTEM 22
3.3.1 Synchronous machine model 23
3.3.2 Single machine infinite bus system eigenvalues and torques 28
3.4 NOVEL CONCEPT TO TUNE POWER SYSTEM STABILIZER 31

3.5 IMPLEMENTATION OF THE DESIGNED PSS ON THE SMIB MODEL 35
3.5.1 Robustness assessment 38
3.6 THE PROCEDURE OF TUNING THE POWER SYSTEM STABILIZER USING OUT OF PHASE TORQUE CORRECTION 40

4. RESULTS AND DISCUSSION 41

4.1 TWO-AREA FOUR-MACHINE SYSTEM 41
4.1.1 Eigenvalues and electrical torques analysis 42
4.1.2 Power system stabilizer tuning 45
4.1.3 Performance comparison of two power system stabilizers 47
4.1.4 Robustness assessment 50
4.2 IEEE 9 BUS SYSTEM 51
4.2.1 Eigenvalues and electrical torques analysis 52
4.2.2 Power system stabilizer tuning 54
4.2.3 Performance of the designed PSS 56
4.2.4 Robustness analysis 57
4.3 IEEE 39 BUS SYSTEM 58
4.3.1 Eigenvalue analysis 58
4.3.2 Power system stabilizer tuning 60
4.3.3 Performance comparison 63

5. CONCLUSION 66

REFERENCES 68

APPENDIX

A. EXPRESSIONS FOR MATRICES $\boldsymbol{G_1(s)}$ TO $\boldsymbol{G_6(s)}$ 70

B. TWO-AREA FOUR-MACHINE SYSTEM DATA TABLES 72

C. IEEE 9-BUS SYSTEM DATA TALBES 75

VITA 78

LIST OF TABLES

3.1 The Eigenvalues and Damping Ratios of the System with No PSS Installed 28

3.2 The Eigenvalues and Damping Ratios Before and After Applying the PSS 36

3.3 Loading Conditions Cases 39

4.1 Eigenvalues and Damping Ratios Obtained from Both Models 44

4.2 Tuned PSS Parameters 46

4.3 System Modes After Applying the Designed PSS 46

4.4 Different Loading Conditions Cases 51

4.5 System Modes and Damping Ratio 54

4.6 PSS Calculated Parameters 55

4.7 Modes and Damping Ratios After Applying the Designed PSSs 55

4.8 Different Loading Conditions of the IEEE 9 Bus System 58

4.9 Eigenvalues Obtained from MATLAB and Simulink Models 60

4.10 Power System Stabilizers Tuned Parameters 62

LIST OF FIGURES

2.1 Torque components in phase domain 5

2.2 Heffron and Phillips model of a single machine infinite bus system 6

2.3 Simplified Heffron and Phillips model 7

2.4 Simplified Heffron and Phillips model with a feedback loop K..... 9

2.5 Power system stabilizer path 10

2.6 Equivalent model of [2] 15

2.7 Excitation system equipped with PSS 15

3.1 State space in block diagram representation……..…… 20

3.2 Single machine infinite bus system 23

3.3 Excitation system 24

3.4 Block diagram representation of swing equations..... 25

3.5 The relation between terminal voltage and the direct and quadrature axis quantities..... 26

3.6 The relation between quantities in d-q-0 and X-Y axis 27

3.7 MATLAB Simulink representation of SMIB system with no PSS installed..... 28

3.8 Speed deviation due to increase in mechanical torque with no PSS installed 29

3.9 Electrical torque from speed deviation $\Delta\omega$ 30

3.10 Electrical torque from reference voltage input $\Delta vref$ 30

3.11 Synchronizing and damping torques developed at frequency = 1 Hz or 6.135 rad/sec..... 31

3.12 Electrical torque phase rotation due to the PSS action 33

3.13 Required transfer function of the power system stabilizer 34

3.14 Bode diagram of the designed PSS 35

3.15 Simulink representation of SMIB system with the PSS installed 36

3.16 Pole zero map of SMIB before and after applying the PSS 37

3.17 Bode diagram of SMIB before and after applying the PSS 37

3.18 Speed deviation due to increase in mechanical torque with the PSS installed 38

3.19 Pole zero map of each case 39

4.1 Single line diagram of the two-area four-machine system……..….41

4.2 Machines speed deviations for a fault on the tie-line for 7 cycles..... 42

4.3 Power transferred through the tie line for a fault on the tie-line for 7 cycles 43

4.4 Pole zero map of the system 44

4.5 Structure of the MB-PSS compared to the designed PSS 47

4.6 Bode diagram of the two stabilizers 48

4.7 Pole zero map of the two stabilizers 48

4.8 Speed deviations of the four machines 49

4.9 Active power transferred over the tie line 50

4.10 Pole zero map of each loading case with the designed PSS installed..... 51

4.11 Single line diagram of the IEEE 9 bus system 52

4.12 Speed deviations due to mechanical step change 53

4.13 Generated active power due to mechanical step changes 53

4.14 Speed deviations due to mechanical step change after installing the PSS 56

4.15 Active power due to mechanical step change after installing the PSS 56

4.16 Speed deviations resulting from both designs 57

4.17 Pole zero map of each loading condition 58

4.18 Single line diagram of the IEEE 39 bus system..... 59

4.19 Speed deviations for IEEE 39 generators 61

4.20 System poles before and after applying the designed PSS 63

4.21 Speed deviations due to a fault on bus 14 64

4.22 Pole zero map of both designs 65

CHAPTER 1

INTRODUCTION

1.1 Background

Synchronous machines with large generating capacity and high-gain fast response excitation systems that are connected via long transmission lines exhibit oscillations of small magnitude and low frequency that often persist for long periods of time. These oscillations place limitations on power transfer capability and can endanger the small signal stability of the system. The Western Interconnection disturbance on August 1996 [1], for example, was caused by poorly damped inter-area oscillations.

Power system stabilizers (PSS) are used to enhance system stability and mitigate the oscillations. A well-tuned PSS helps in damping rotor oscillations caused by small disturbances through generating a component of electrical torque in phase with the speed variations.

1.2 Problem Statement

Designing a power system stabilizer in a multimachine environment has received special attention since it helps in improving the damping ratio of the oscillatory modes. Recent schemes focused on employing the single machine infinite bus method on a multimachine system [2], [3] by assuming the resulting network admittance matrix is diagonally dominant, hence, all the information needed to design a power system stabilizer is extracted locally. However, these methods do not to provide accurate information about the PSS gain, also, the designed PSS

performance on some test systems is poor, as these systems are characterized by non-diagonal network admittance matrix.

1.3 Objective

This work aims to develop a robust PSS design that provides damping torque by correcting the phase of generators electrical torques with a simplified tuning process that assumes identical stages and a fixed ratio between the lead/lag time constants.

1.4 Study Outline

- Chapter 2: this chapter explains the small signal stability problem and reviews the power system stabilizer tuning methods.
- Chapter 3: outlines the theory of small signal stability, generator electrical torques, formulation of the tuning method, and its implementation on the single machine infinite bus system.
- Chapter 4: in this chapter, the simulation results when implementing the developed method on a several test systems are presented. Furthermore, comparisons between the proposed method and other methods that follow different designing techniques are shown. Finally, robustness assessment is carried out to validate the effectiveness of the proposed method.
- Chapter 5: this chapter recapitulates the advantages of the developed method.

CHAPTER 2

LITERATURE REVIEW

2.1 Introduction

Due to the increased efforts to transmit power through long high-voltage transmission lines to satisfy the increasing demand in modern cities, certain instability concerns regarding a major fault or disturbance have increased. In particular, generators may fall out of step due to insufficient synchronizing torque. To remedy this problem high-gain fast-acting excitation systems are introduced. Although high-gain excitation systems help the synchronizing torque problem, they introduce negative damping to certain electromechanical modes.

To remove the constraints placed on the regulator gain an auxiliary controller called power system stabilizer (PSS) is introduced. The power system stabilizer uses a special stabilizing signal derived from the machine speed, terminal frequency, or power. The main role of the PSS is to provide damping to the electro-mechanical modes. Pure damping occurs when the induced electrical torque is in-phase with speed variations. Therefore, the compensation transfer function provided by the PSS must be properly designed to introduce such a torque on the shaft of the generator.

2.2 Rotor Angle Stability

Rotor angle stability refers to the ability of a synchronous machine of an interconnected system to remain in synchronism after being subjected to a disturbance [4]. The system is stable when a new equilibrium point between electromagnetic torque and mechanical torque is

restored/maintained in each synchronous machine in the system after subjected to a disturbance. Instability occurs when angular swings increase, thus, lead to loss of synchronism.

Rotor angle stability can be divided into two subcategories:

- Small-signal rotor angle stability is defined as the ability of the power system to maintain synchronism under small disturbances.
- Large-disturbance rotor angle stability (transient stability) describes the ability of the power system to maintain synchronism after being subjected to a severe disturbance.

The change in electromagnetic torque of a synchronous machine following a disturbance can be broken down into two components:

(i) Synchronizing torque: in-phase with rotor angle deviation.

(ii) Damping torque: in-phase with speed deviations.

$$\Delta T_e = K_s.\Delta\delta + K_d.\Delta\omega \qquad 2.1$$

Small-signal stability problems occur in a form of increasing rotor oscillations due to insufficient damping torque. In contrast, in transient stability, instability comes in a form of aperiodic angle separation occurs due to insufficient synchronizing torque.

Under normal operating conditions both components are positive K_s, K_d , therefore, a change in rotor's speed or angular position produces electrical torque that acts on the rotor to restore equilibrium.

The effect of these torques on machine stability can be examined by the phase plane diagram shown in Figure 2.1. Note that in the phase-domain speed deviation $\Delta\omega$ leads angle deviation $\Delta\delta$ by 90 degrees.

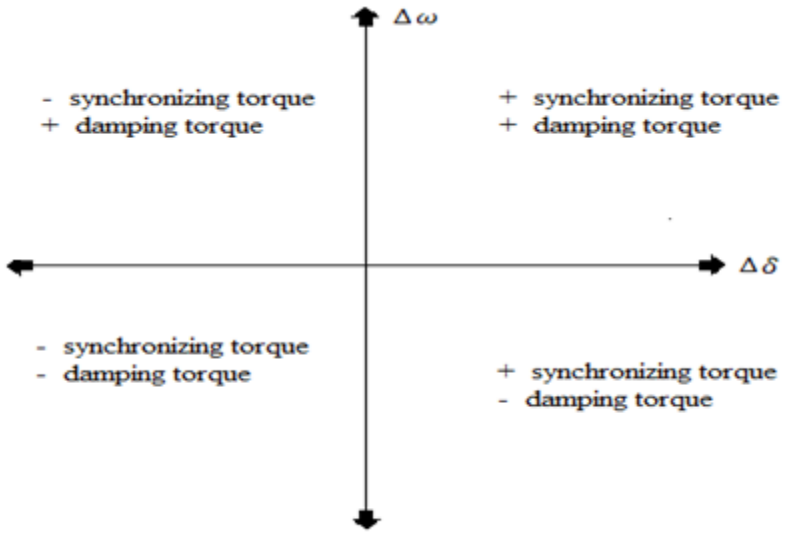

Figure 2.1 Torque components in phase domain

Figure 2.1 indicates that electrical torques that are in-phase with speed deviations and angle deviations increase damping and synchronizing torque, respectively.

The rotor angle stability of synchronous machine can be studied further with the aid of block diagram relating electromagnetic torque, speed, and angle [5] [6].

2.3 Heffron and Phillips Model of Single Machine-Infinite Bus System

The linearized model of a single machine connected to an infinite bus (SMIB) developed by Heffron and Phillips [5] can be used to deepen the understanding of synchronizing and damping torques. It includes a third-order representation of the synchronous machine and a first order model of the excitation system as shown in Figure 2.2. The constants K_1 to K_6 depend on the operating conditions as well as external system impedance and can be found on reference [6].

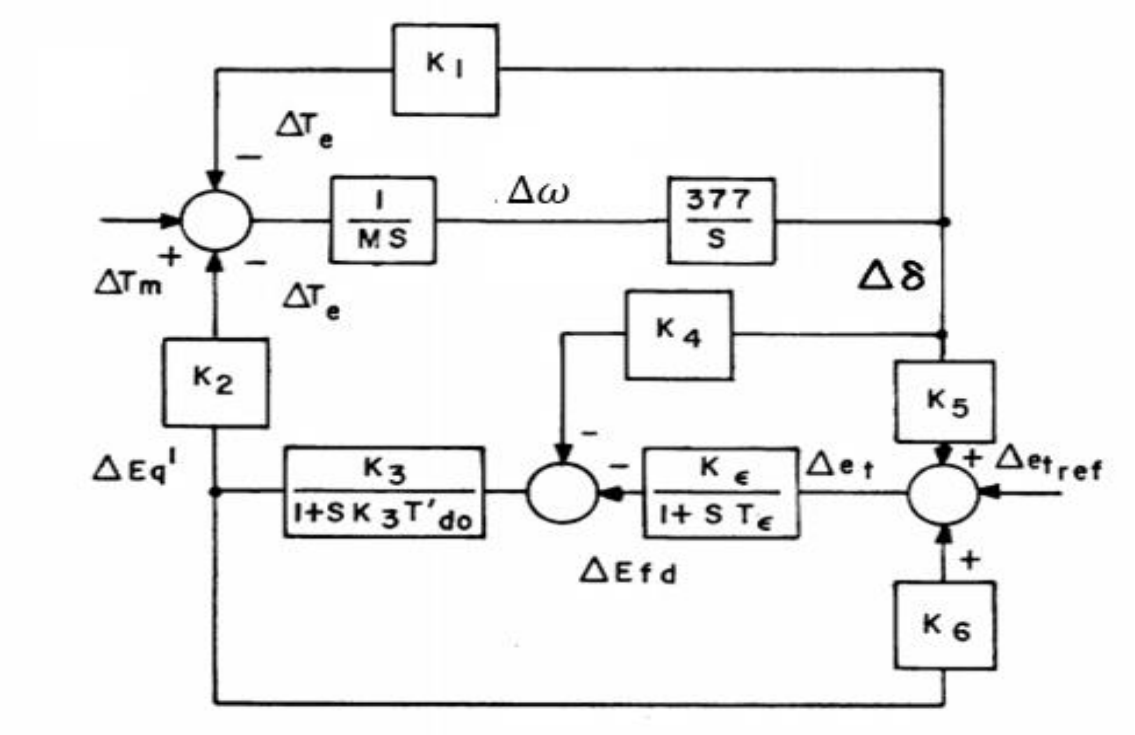

Figure 2.2 Heffron and Phillips model of a single machine infinite bus system

A simplified second order model shown in Figure 2.3 can be obtained by assuming the following:

(i) There are no perturbations in reference voltage Δe_{ref}

(ii) Damping coefficient D that provides a torque in phase with speed deviations.

(iii) The exciter and open circuit time constants $T_\epsilon \; and \; K_3 T'_{do}$ are very short.

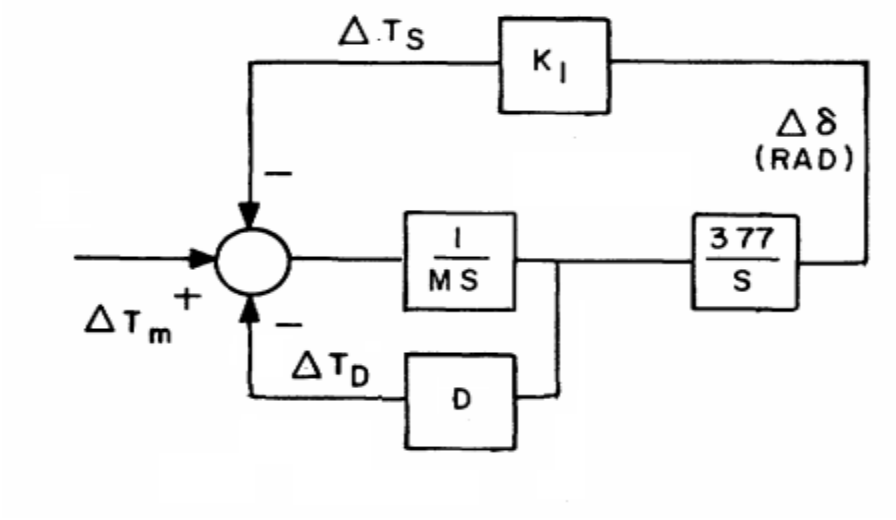

Figure 2.3 Simplified Heffron and Phillips model

This simplified model, in fact, can be seen as a manifestation of the swing equation in terms of block diagrams, with $K_1.\Delta\delta$ as the synchronizing torque K_s, and $D.\Delta\omega$ as the damping torque K_d; hence, it can be represented by the following equation:

$$\frac{d\,\Delta\omega}{dt} = \frac{1}{M}(\Delta T_m - K_s.\Delta\delta - K_d.\Delta\omega) \qquad 2.2$$

Where

$$\frac{d\,\Delta\delta}{dt} = \omega_0 \Delta\,\omega$$

By substituting M = 2H, the resulting characteristics equation in S-domain from the simplified model in Figure 2.2 can be expressed as:

$$s^2 + \frac{D}{2H}.s + \frac{K_1.\omega_0}{2H} = 0 \qquad 2.3$$

The roots of this system s_1, s_2 are a pair of complex poles located at:

$$s_1, s_2 = -\frac{D}{4H} \pm j\frac{1}{2}\sqrt{\frac{4\omega_0 K_1}{2H} - (\frac{D}{2H})^2} \qquad 2.4$$

When $D \ll 4\omega_0 K_1$ these roots exhibit damped oscillatory nature with a frequency $\omega_n = \sqrt{\frac{4\omega_0 K_1}{2H}}$, and damping ratio $\zeta = \frac{1}{2}(\frac{D}{\sqrt{2K_1\omega_0 H}})$. For typical ranges of inertia, impedances, and loading conditions, the frequency of oscillations ranges between 0.1 and 2 Hz,

2.3.1 The effect of excitation system on damping torque

By examining the path between $\Delta\delta$ and ΔT_e through the exciter in Figure 2.2, we can write the transfer function as follows [6]:

$$\frac{\Delta T_e}{\Delta\delta} = -\frac{K_2 K_\epsilon K_5}{\left(\frac{1}{K_3} + K_\epsilon K_6\right) + s\left(\frac{K_\epsilon}{K_3} + T'_{d0}\right) + s^2 T'_{d0} T_\epsilon} \quad 2.5$$

Realizing that $K_\epsilon \gg 1$, for very low frequencies, Equation 2.5 can be simplified to:

$$\Delta T_e = -\frac{K_2 K_5 \Delta\delta}{K_6} \quad 2.6$$

Note that the effect of this expression on synchronizing torque is determined by K_5. When K_5 is negative (e.g. heavy loading conditions), the synchronizing torque is positive, thus, contribute to system stability.

The expression in 2.5 also produces a damping torque component given by:

$$\Delta T_e = \frac{K_2 K_\epsilon K_5 \left(\frac{K_\epsilon}{K_3} + T'_{d0}\right)\omega}{\left(\frac{1}{K_3} + K_\epsilon K_6 - \omega^2 T'_{d0} T_\epsilon\right) + (\frac{T_\epsilon}{K_3} + T'_{d0})^2\omega^2}\,\Delta\delta \quad 2.7$$

According to expression 2.7, the exciter – while producing positive synchronizing torque for negative values of K_5 – it produces negative damping torque, hence, affect the stability of the machine. Note, also, the magnitude of negative damping is proportional to the exciter gain K_ϵ.

One way to reconcile these two conflicting requirements is to provide damping torque using an auxiliary controller (power system stabilizer). A power system stabilizer removes the

constraints placed on exciter gain K_ϵ, at the same time, it provides the required damping torque by modulating the voltage reference in response to speed deviation.

2.3.2 The role of the power system stabilizer

The role of an ideal power system stabilizer can be illustrated using the simplified second order model in Figure 2.3. Let us assume that we can add a feedback loop with a gain K as shown in Figure 2.4 such that $\Delta T_{DK} = K.\Delta\omega$.

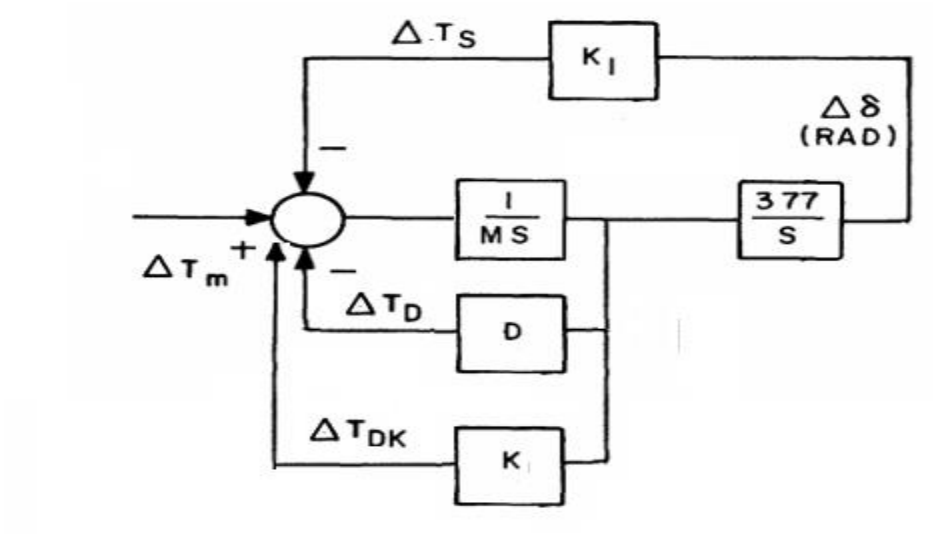

Figure 2.4 Simplified Heffron and Phillips model with a feedback loop K

This gain K affects the location of the poles of the characteristics equation given in Equation 2.3 by introducing a direct left-shift, therefore, the new poles location is at $-(K + D)/4H$.

In practice, the power system stabilizer output is applied to the exciter summation junction to modulate the reference voltage. This path at which the PSS is added exhibits frequency dependency characteristics, in fact, it produces a phase lag due to the exciter and machine time constants. This path is indicated by the transfer function Gp(s) as shown in Figure 2.5.

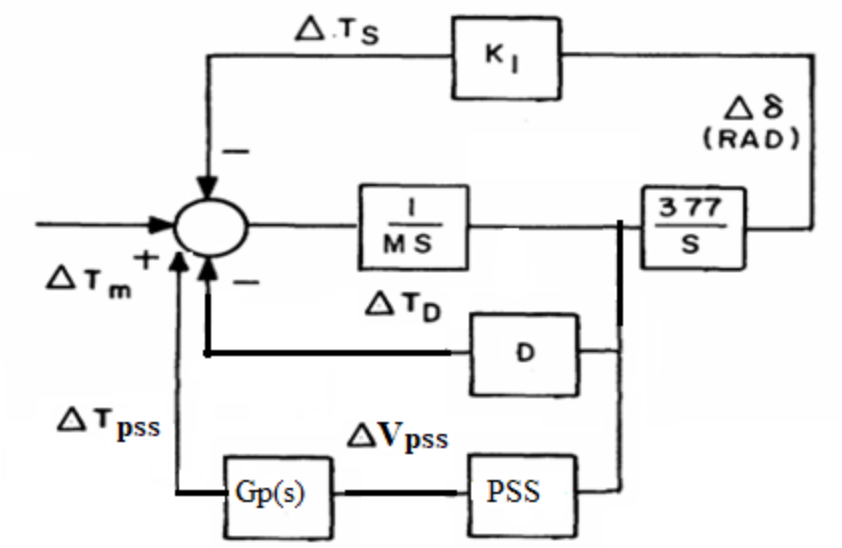

Figure 2.5 Power system stabilizer path

For the PSS in Figure 2.5 to produce torques that are in-phase with speed deviations i.e. damping torque, the PSS transfer function must compensate for the phase lag caused by the transfer function Gp(s). Hence, designing a power system stabilizer requires a thorough study of this transfer function.

In literature, several methods have been developed to design the power system stabilizer. One of the famous methods [6] uses frequency response analysis to determine the transfer function between the stabilizing signal and electric torque. The PSS is then designed to compensate for the phase lag and the magnitude caused by this transfer function. The following section provides a brief description of PSS design using frequency response analysis.

2.4 Power System Stabilizer Designing Approaches

Several approaches have been used to design the power system stabilizer. The paper by de Mello and Concordia [6] presented the basis of power system stabilizer design. In their approach, the PSS transfer function is designed to provide the phase compensation for the transfer function

between the electrical torque and the voltage reference input to the AVR. This transfer function is also called the generator, the excitation system, and the power system $GEP(j\omega)$. It is nearly identical to the closed loop voltage regulator transfer function, which can be measured by changing the input of the reference voltage and monitor the terminal voltage of the machine.

$$GEP(j\omega) = \frac{V_t(j\omega)}{V_{ref}(j\omega)} \qquad 2.8$$

The power system stabilizer is tuned to provide the required phase compensation for this transfer function over the range of interest. The optimum gain is set to equal one third of the instability gain.

In a different approach for multi-machine system, reference [7] observes that the transfer function between the voltage reference and the electrical power $P - V_r(j\omega)$with all rotor shaft dynamics disabled (by setting $\Delta\delta$=0) agrees closely to the $GEP(j\omega)$. The PSS is designed to compensate for the lag caused by this function. Therefore, for machine j the PSS functions $\mathrm{G_j}(\mathrm{j}\omega)$ is the reciprocal of $(P - V_r(\mathrm{j}\omega))_j$, hence:

$$\mathrm{G_j}(\mathrm{j}\omega) = \frac{1}{(P - V_r(\mathrm{j}\omega))_j} \qquad 2.9$$

To introduce left shift for the mode of interest $\lambda_{h,}$ the compensation angle of the PSS should be 180 degrees from the $P - V_r(j)$:

$$\arg\{\mathrm{G_j}(\mathrm{j}\omega)\} = -\arg\{(P - V_r(\mathrm{j}\omega))_j\} \qquad 2.10$$

Motivated by the work in [7], Lam et. al [8] conducted a thorough analysis of the frequency response of generator electrical torque in a multi-machines environment. The analysis uses operational matrix technique [9], with shaft dynamic disabled as in [7], and no change in mechanical torque ΔT_m.

In their model, a generator with an AVR reference input v_{ref} is described by the following set of equations:

$$2H\ s\Delta\omega + D.\Delta\omega = -\Delta T_e \quad 2.11$$

$$s\Delta\delta = \omega_0\Delta\omega \quad 2.12$$

$$\Delta E_{fd} = G_{avr}(s).(\Delta v_{ref} - \Delta v_t) \quad 2.13$$

$$v_{t0}\Delta v_t = v_{d0}\Delta v_d + v_{q0}\Delta v_q \quad 2.14$$

$$\Delta T_e = \Delta i_{d0}\Delta v_d + \Delta i_{q0}\Delta v_q + v_{d0}\Delta i_d + v_{q0}\Delta i_q \quad 2.15$$

$$\begin{bmatrix}\Delta v_d \\ \Delta v_q\end{bmatrix} = \begin{bmatrix}0 & x_q(s) \\ -x_d(s) & 0\end{bmatrix}\begin{bmatrix}\Delta i_d \\ \Delta i_q\end{bmatrix} + \begin{bmatrix}0 \\ G(s)\end{bmatrix}\Delta E_{fd} \quad 2.16$$

Where,

s : complex frequency.

$v_d, v_q, i_d, i_q, x_d(s)\ and\ x_q(s)$: d and q axis voltages, currents and operational impedances, respectively.

H : the machine inertia. D : damping coefficient.

$G(s)$: Generator transfer function.

$G_{avr}(s)$: exciter transfer function.

E_{fd}: field voltage.

v_t: terminal voltage.

Subscript '0' represents steady state quantities, on the other hand, Δ denotes to perturbed quantities.

Transforming the voltages, and currents from the machine d-q reference to X-Y reference, from Equations 2.12 through 2.16, we obtain the following set of equations on the X-Y reference:

$$\Delta i_g = G_1(s)\Delta v_g + G_2(s)\Delta\omega + G_5(s)\Delta v_{ref} \quad 2.17$$

$$\Delta T_e = G_3(s)\Delta v_g + G_4(s)\Delta\omega + G_6(s)\Delta v_{ref} \quad 2.18$$

Where $\Delta v_g = [\Delta v_x \quad \Delta v_y]^T$ and $\Delta i_g = [\Delta i_x \quad \Delta i_y]^T$ are the generator voltage and currents in the X-Y coordinates, matrices $G_1(s)$ to $G_6(s)$ are given in Appendix A.

Recall the network equation (Ohm's law):

$$\Delta i = Y\Delta v$$

Where the admittance matrix Y is split into real and imaginary parts, e.g. for n nodes system, the dimension of Y is $2n \times 2n$. From Equations 2.17 to 2.18 we can obtain an expression for generator electrical torque as follows:

$$\Delta T_e = K(s)\Delta\omega + L(s)\,\Delta v_{ref} \quad 2.19$$

$$K(s) = G_3(s).Y_e^{-1}(s).G_2(s) + G_4(s) \quad 2.20$$

$$L(s) = G_3(s).Y_e^{-1}(s).G_5(s) + G_6(s) \quad 2.21$$

$$Y_e^{-1}(s) = (Y - G_1(s)) \quad 2.22$$

The expressions in 2.19 to 2.21 are valid for multimachine system, with minor modifications on the Y matrix. First, system loads are modeled as static load, hence, can be absorbed into the Y matrix, afterwards, the matrix is reduced to generators terminals.

Frequency response can be obtained by substituting $s = j\omega$ in 2.20 and 2.21. For each generator, the diagonal elements of $L(s)$ gives the transfer function required to design the PSS. The diagonal elements of $K(s)$ identifies the generators with negative or insufficient damping torque. Finally, $Y_e^{-1}(s)$ is the system admittance matrix reduced to generators terminals, including each generator dynamic admittance $G_1(s)$.

According to [8], the modified admittance matrix $Y_e^{-1}(s)$ was found to be diagonally dominant, suggesting that $L(s)$ is also diagonally dominant, thus, designing power system stabilizer can be achieved using single machine infinite bus method in multimachine system.

Based on the analysis provided by [8], reference [3] proposed a designing technique using local measurements obtained from generators' plant by taking the transformer high voltage bus as a voltage instead of infinite bus. SMIB Constants K_1 to K_6 [5] are modified to include the transformer high voltage bus. The design calculates the $GEP(j\omega)$ based on the new constants, the gain is selected by plotting the root locus with slip speed as output, such that the damping ratio of the rotor mode is maximized.

Following the same line of analysis, [2] proposed a design method involving local measurements, however, a major difference from the method proposed in [3] is that [2] went beyond the transformer high voltage bus, and used the equivalent voltage and impedance of the transmission lines emanating from the transformers' high voltage bus, as shown in Figure 2.6

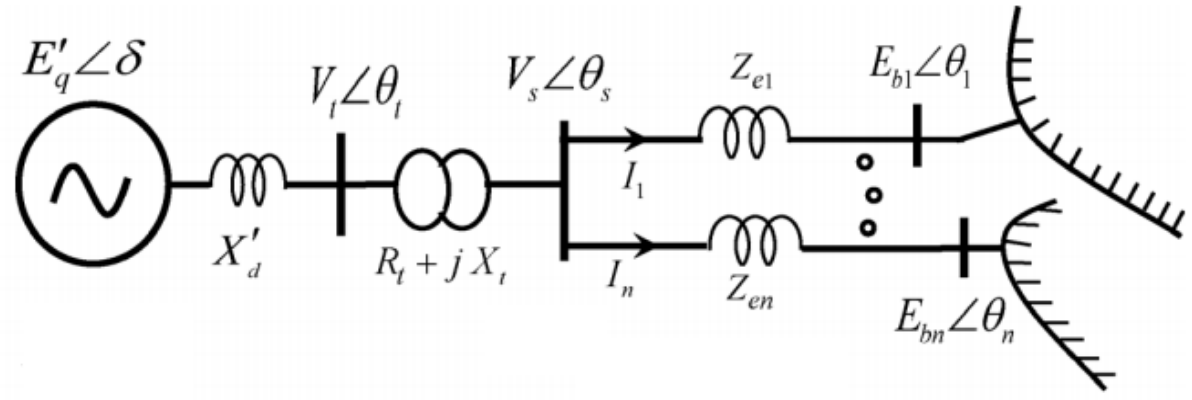

Figure 2.6 Equivalent model of [2]

2.5 Power System Stabilizer Tuning Concepts

Power system stabilizer consists of a washout stage, and a number of lead/lag blocks that depends on the compensation required, usually 2 stages are sufficient to provide the desired phase compensation as shown in Figure 2.7. The washout time constant is set at 10 seconds such that it filters out low frequency and produces no impact upon the local modes.

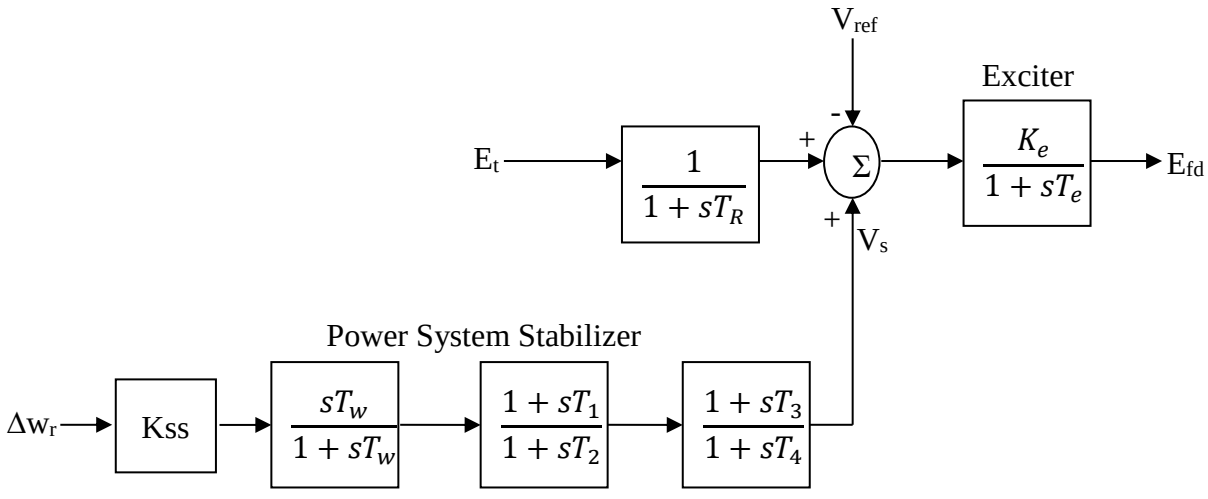

Figure 2.7 Excitation system equipped with PSS

A 10:1 spread ratio between the lead and lag time constants is proposed by [10], which gives a maximum compensation frequency $f_c\ rad/sec$ at:

$$f_c = \frac{\sqrt{10}}{T_1} \qquad 2.23$$

Pure positive damping to a mode occurs with perfect compensation - i.e. the phase lead characteristics of the PSS cancel out the lag characteristics of the plant through which the stabilizer operates - the mode will move directly to the left-hand side of the s-plane. If phase lag θ exists, the change in modes' frequency $\Delta\omega_m$ due to change in damping $\Delta\sigma_m$ is governed by:

$$\Delta\omega_m = -\tan(\theta).\Delta\sigma_m \qquad 2.24$$

CHAPTER 3

METHODOLOGY

A power system stabilizer is a device that modulates the exciter reference voltage to provide damping torque to rotor oscillatory modes produced by small disturbances. These oscillatory modes usually range between 0.6 to 12.5 rad/sec (0.1- 2 Hz). The basic function of the power system stabilizer is to provide positive damping in this range of frequencies by producing an electrical torque in-phase with the rotor speed deviations.

This work presents a new method to tune the parameters of the power system stabilizer to provide such positive damping torque. The tuning process of the power system stabilizer is simplified to tune only two parameters PSS gain, and one time constant by assuming identical stages and a fixed ratio between the lead-lag time constants.

Unlike the methods described in Chapter 2, which depend on local measurements to design a power system stabilizer in a multimachine system, this method rather includes system information through a modified system admittance matrix and calculates the frequency responses of each generator's electrical torques. The calculated torques were found to have large imaginary component that do not contribute to damping. The power system stabilizer is tuned to correct the out of phase torques, thus provide positive damping torque.

The next section gives a brief background of state space models and eigenvalues. Section 3.2 explains the generators' electrical torques. Section 3.3 illustrates the torques developed in a single machine infinite bus system. Section 3.4 describes the novel concept of tuning the PSS.

Application of the proposed method on the SMIB system is found in Section 3.5. Finally, proposed procedure to tune the PSS is presented in Section 3.6.

3.1 Background

3.1.1 State space models

State space model represents the mathematical model of a dynamic system as a set of inputs, outputs, and state variables related by first order differential equations. State variables define the minimum number of variables at time t_0 that are required to describe the response of the system in the future. Hence, the power system dynamic behavior can be described using state space by a set of n nonlinear differential equations as follows:

$$\dot{x} = f(x, u) \tag{3.1}$$

$$x = \begin{bmatrix} x_1 \\ \vdots \\ x_n \end{bmatrix} \qquad u = \begin{bmatrix} u_1 \\ \vdots \\ u_r \end{bmatrix}$$

Where:

x is the state vector with dimensions n×1 to indicate the system order. and u is the input vector which contains r inputs.

Likewise, Observable m×1 outputs of the system can be expressed in terms of state variables and the input by the following form.

$$y = g(x, u) \tag{3.2}$$

3.1.2 Equilibrium points and linearization

Equilibrium points are the points where all the n first order differential equations described in Equation 3.1 are simultaneously zero, thus:

$$f(x_0) = 0 \tag{3.3}$$

Equation 3.3 can be linearized around an equilibrium point x_0 as follows:

$$\dot{x} = \dot{x}_0 + \Delta\dot{x}$$

$$= f[(x_0 + \Delta x), (u_0 + \Delta u)] \quad 3.4$$

Where:

$$\dot{x}_0 = f(x_0, u_0)$$

$x_{0,}$ and u_0 are the initial state vector and the input vector at the equilibrium point, respectively.

Using Taylor's series expansion and ignoring higher derivatives, we find:

$$\dot{x}_i = \dot{x}_{i0} + \Delta\dot{x}_i = f_i[(x_0 + \Delta x), (u_0 + \Delta u)]$$

$$= f_i(x_0 + u_0) + \frac{\partial f_i}{\partial x_1}\Delta x_1 + \cdots + \frac{\partial f_i}{\partial x_n}\Delta x_n + \frac{\partial f_i}{\partial u_1}\Delta u_1 + \cdots + \frac{\partial f_i}{\partial u_n}\Delta u_n \quad 3.5$$

$$\Delta y_i = \frac{\partial g_j}{\partial x_1}\Delta x_1 + \cdots + \frac{\partial g_j}{\partial x_n}\Delta x_n + \frac{\partial g_j}{\partial u_1}\Delta u_1 + \cdots + \frac{\partial g_j}{\partial u_r}\Delta u_r \quad 3.6$$

By looking at Equations 3.5 and 3.6, small changes in state variables derivatives and outputs can be expressed by Equations 3.7 and 3.8 as follows:

$$\Delta\dot{x}_i = \frac{\partial f_i}{\partial x_1}\Delta x_1 + \cdots + \frac{\partial f_i}{\partial x_n}\Delta x_n + \frac{\partial f_i}{\partial u_1}\Delta u_1 + \cdots + \frac{\partial f_i}{\partial u_r}\Delta u_r \quad 3.7$$

$$\Delta y_i = \frac{\partial g_j}{\partial x_1}\Delta x_1 + \cdots + \frac{\partial g_j}{\partial x_n}\Delta x_n + \frac{\partial g_j}{\partial u_1}\Delta u_1 + \cdots + \frac{\partial g_j}{\partial u_r}\Delta u_r \quad 3.8$$

In matrix form, the above expression can be written as:

$$\Delta\dot{x} = A\Delta x + B\Delta u \quad 3.9$$

$$\Delta y = C\Delta x + D\Delta u \quad 3.10$$

Where A contains the derivatives of f_i with respect to x_i. B comprises the derivatives of f_i by u_i. Same case for C and D matrices, however, f_i is substituted by g_i.

Above equations can be mapped into the frequency domain as follows:

$$s\Delta x(s) - \Delta x(0) = A\Delta x(s) + B\Delta u(s) \quad 3.11$$

$$\Delta y(s) = C\Delta x(s) + D\Delta u(s) \quad 3.12$$

Assuming zero initial conditions, the block diagram in Figure 3.1 can be used to represent Equations 3.11 and 3.12.

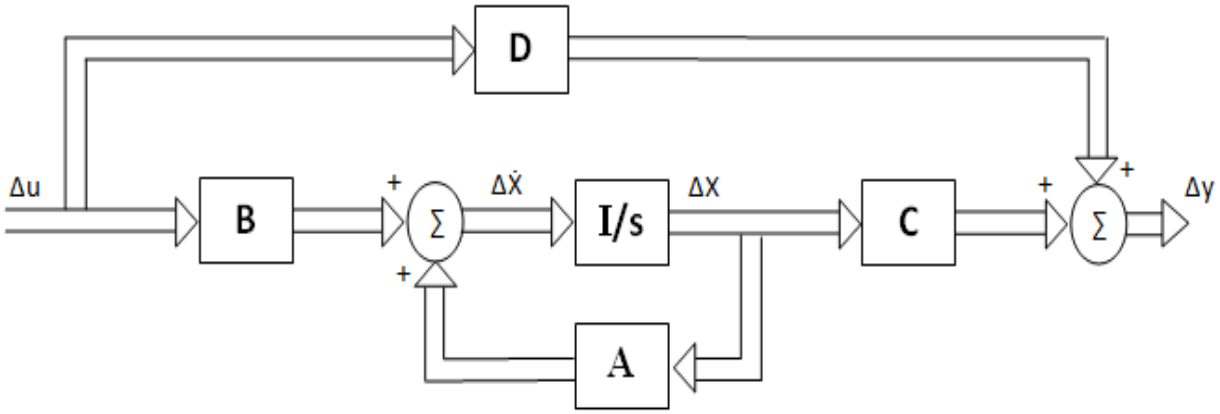

Figure 3.1 State space in block diagram representation

Solving for Δx(s):

$$(sI - A)\Delta x(s) = \Delta x(0) + B\Delta u(s) \quad 3.13$$

Then

$$\Delta x(s) = (sI - A)^{-1}[\Delta x(0) + B\Delta u(s)] \quad 3.14$$

$$= \frac{adj(sI - A)}{\det(sI - A)}[\Delta x(0) + B\Delta u(s)] \quad 3.15$$

And

$$\Delta y(s) = C\frac{adj(sI - A)}{\det(sI - A)}[\Delta x(0) + B\Delta u(s)] + D\Delta u(s) \quad 3.16$$

The poles of the system can be obtained by solving the characteristic equation of the system given by Equation 3.17:

$$\det(sI - A) = 0 \quad 3.17$$

3.1.3 Eigenvalues

Eigenvalues are defined as the values of the scalar parameter λ the gives a non-trivial solution of the equation below [11]:

$$A\phi = \lambda\phi \tag{3.18}$$

Where A is a nxn matrix and ϕ is a nx1 vector.

Equation 3.18 can be written in the form:

$$(A - \lambda I)\phi = 0 \tag{3.19}$$

Now solve:

$$det(A - \lambda I) = 0 \tag{3.20}$$

Solving Equation 3.20 yields the n eigenvalues of the state matrix A.

3.2 Generator Electrical Torques

Recall Equation 2.19 from Chapter 2. Lam [8] defined the electrical torques as a function of speed deviations $\Delta\omega$ and the AVR reference voltage Δv_{ref} as follows:

$$\Delta T_e = K(s)\Delta\omega + L(s)\,\Delta v_{ref} \tag{3.21}$$

$$K(s) = G_3(s).Y_e^{-1}(s).G_2(s) + G_4(s) \tag{3.22}$$

$$L(s) = G_3(s).Y_e^{-1}(s).G_5(s) + G_6(s) \tag{3.23}$$

By ignoring the electrical torque due to AVR reference voltage, Equation 3.21 can be expressed as:

$$\Delta T_e = K(s)\Delta\omega \tag{3.24}$$

Expression 3.24 has two components real and imaginary, therefore can be written in the formula:

$$\Delta T_e = real\big(K(s)\big).\Delta\omega + imag\big(K(s)\big).\Delta\omega \quad (3.25)$$

also note that generators' electrical torque can be broken into two components as follows:

$$\Delta T_e = K_s.\Delta\delta + K_d.\Delta\omega \quad (3.26)$$

$$\frac{d\,\Delta\delta}{dt} = \omega_0 \Delta\,\omega \quad (3.27)$$

Where:

K_s, K_d are the synchronizing and damping torques due to change in speed, respectively.

$\Delta\delta$ is the angle deviation, and ω_0 is the nominal speed.

Equation 3.27 can be transformed to the phase-domain by substituting j = $\frac{d}{dt}$ as follows:

$$\Delta\delta = \frac{\omega_0\Delta\omega}{j} \quad (3.28)$$

Now substituting Equation 3.28 into 3.26:

$$\Delta T_e = K_s.\frac{\omega_0.\Delta\omega}{j} + K_d.\Delta\omega \quad (3.29)$$

Finally, Equation 3.29 becomes:

$$\Delta T_e = -jK_s.\omega_0.\Delta\omega + K_d.\Delta\omega \quad (3.30)$$

Comparing Equation 3.25 and 3.30 we find that the imaginary part of $K(s)$ corresponds to synchronizing torque. On the other hand, the real part gives the damping torque. Thus, any positive torque in-phase with speed deviations produces a positive damping torque. In contrast, any positive torque 90 degrees lagging on speed deviations produces a positive synchronizing torque.

3.3 Single Machine Infinite Bus System

Single machine infinite bus mentioned in Kundur example 12.3[10] is used to demonstrate the concept of both small signal stability, and electrical torques, is shown in Figure 3.2.

Figure 3.2 Single machine infinite bus system

3.3.1 Synchronous machine model

To analyze the small signal stability of the system given in Figure 3.2, the synchronous machine is represented by a simplified model where effects of stator transients and speed variations on power are neglected. This is simplification allows the use of steady state relationship, hence, transmission network equations can be added. Moreover, constant speed permits the interchange between the per unit power and torque.

The dynamics of power system for small signal stability can be described by two set of equations. One set that describes the differential equations associated with synchronous machine also known as system state variables, and algebraic equations or non-state variables that represent other system components such as transmission lines.

1. State variables:

For small disturbance analysis, the synchronous machine is described by four state variables as follows:

(i) Voltage behind transient reactance(X'_d) equation E'_q

In the d-q-0 reference frame, this voltage can be expressed as:

$$pE'_q = \frac{1}{T'_{d0}}[-E'_q - (X_d - X'_d)i_d] \qquad 3.31$$

Where E'_q is the q-axis component of the voltage behind transient reactance X'_d

T'_{d0} is the open circuit transient time constant

E_{fd} is the field circuit voltage

X_d and X'_d are the direct axis reactance, and transient reactance, respectivley.

I_d is the direct axis current

For small disturbance analysis Equation 3.31 becomes:

$$\Delta \dot{E}'_q = \frac{1}{T_{d0}} [\Delta E_{fd} - \Delta E'_q - (X_d - X'_d).\Delta I_d] \quad 3.32$$

(ii) Field voltage equation

Figure 3.3 shows the model of the exciter that is used. The output $\dot{E_{fd}}$ can be expressed by the Equation 3.33

$$\dot{E_{fd}} = \frac{1}{T_e} [(K_e(v_{ref} - V_t) - E_{fd}] \quad 3.33$$

Where K_e, T_e are the exciter gain and time constant respectively.

V_{ref} is the voltage reference setting point.

V_t is the machine terminal voltage

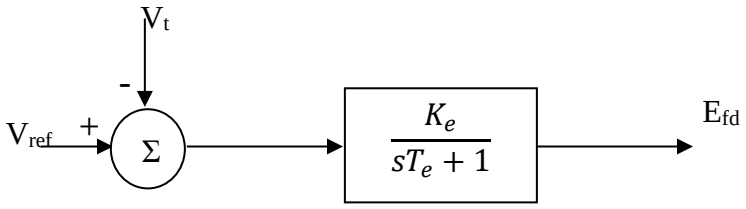

Figure 3.3 Excitation system

The perturbed Equation of 3.33 can be expressed as:

$$\Delta\dot{E}_{fd} = \frac{1}{T_e}\left(-K_e\Delta V_t - \Delta E_{fd}\right) \quad 3.34$$

(iii) Swing equations

Changes in electrical state of the system affect the rotation of the machine. Thus, cause electro-mechanical oscillations. The Swing equation describes the difference between the electrical torque, mechanical torque, and damping torque of the machine as follows:

$$\frac{d\,\omega_r}{dt} = \frac{1}{2H}(T_m - T_e - K_D\Delta\,\omega_r) \quad 3.35$$

$$\frac{d\,\delta}{dt} = \omega_0\Delta\omega_r \quad 3.36$$

Since speed is assumed to be constant, P_m and P_e may be used in place of T_m and T_e. These equations can be linearized as shown below:

$$\frac{d\,\Delta\omega_r}{dt} = \frac{1}{2H}(P_m - P_e - K_D\Delta\,\omega_r) \quad 3.37$$

$$\frac{d\Delta\delta}{dt} = \omega_0\Delta\omega_r \quad 3.38$$

The block diagram of Figure 3.4 represents the swing equations.

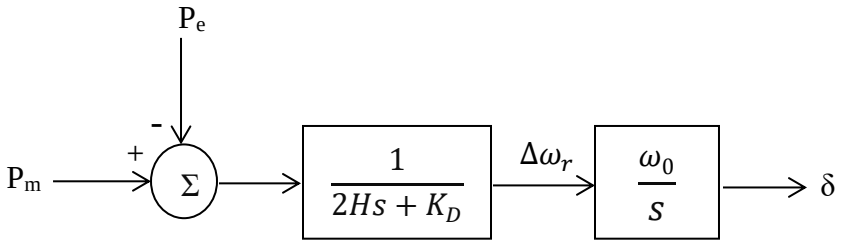

Figure 3.4 Block diagram representation of swing equations

2. Non-state variables:

To complete the modelling of the dynamic system to include all system components, nine additional non-state variables were temporarily used as intermediate variables (V_t, V_d, V_q, I_d, I_q, V_x, V_y, I_x and I_y).

The machine terminal voltage is related to the machine direct and quadrature currents, and voltages through the phasor diagram shown in Figure 3.5, hence, the following perturbed equation can be obtained:

$$0 = -\Delta V_d + X_q.\Delta I_q \tag{3.39}$$

$$0 = -\Delta V_q + \Delta E'_q - X'_d.\Delta I_d \tag{3.40}$$

$$0 = -\Delta V_t + \frac{E_q}{V_t}.\Delta V_q + \frac{E_d}{V_t}.\Delta V_d \tag{3.41}$$

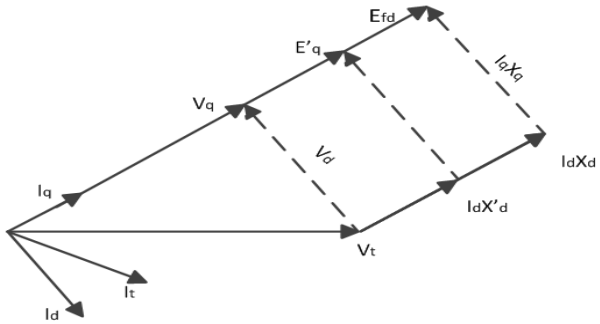

Figure 3.5 The relation between terminal voltage and the direct and quadrature axis quantities

To couple the machine voltages and current to the network equation. These values are to be transformed from the d-q reference to the X-Y reference as shown in Figure 3.6. As a result, four equations are formed as follows:

$$0 = -\Delta I_d + I_q \Delta\delta + sin\ \delta \Delta I_x - \cos\delta \Delta I_y \quad 3.42$$

$$0 = -\Delta I_q + I_d \Delta\delta + cos\ \delta \Delta I_x + \sin\delta \Delta I_y \quad 3.43$$

$$0 = -\Delta V_x - V_y \Delta\delta + sin\ \delta \Delta V_d + \cos\delta \Delta V_q \quad 3.44$$

$$0 = -\Delta V_y + V_x \Delta\delta + cos\ \delta \Delta V_d + \sin\delta \Delta V_q \quad 3.45$$

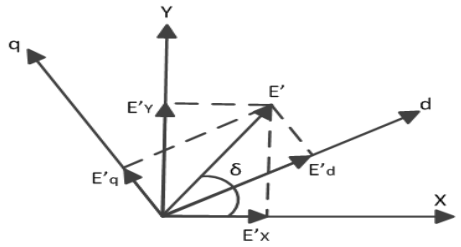

Figure 3.6 The relation between quantities in d-q-0 and X-Y axis

Last two equations are the transmission network equations stated below:

$$0 = -\Delta I_x + \sum_i g_{ij} \Delta V_{xj} - \sum_i b_{ij} \Delta V_{yj} \quad 3.46$$

$$0 = -\Delta I_y + \sum_i b_{ij} \Delta V_{xj} - \sum_i g_{ij} \Delta V_{yj} \quad 3.47$$

Two separate MATLAB scripts were developed to calculate the eigenvalues of the system above, and to find the frequency response of machines' electrical torques given by Equations 3.22 and 3.23. Figure 3.7 shows the MATLAB Simulink model that has been constructed by using equations defined in Section 3.3.1.

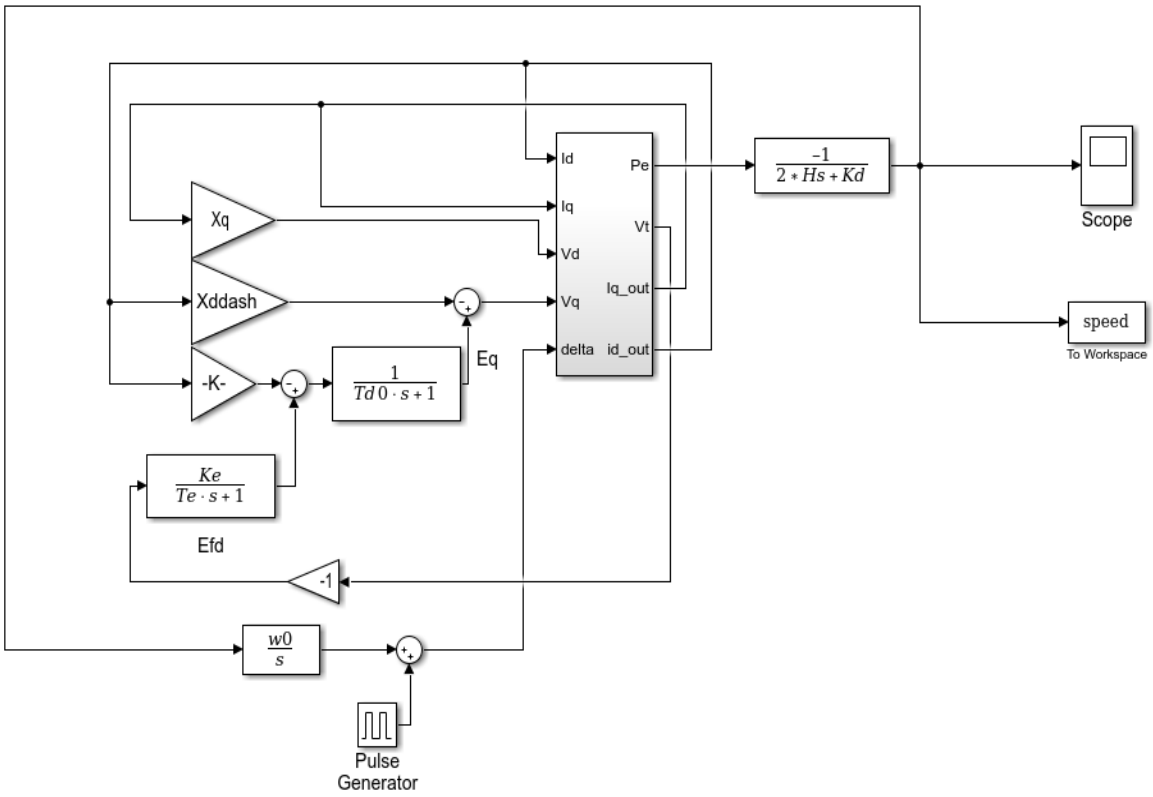

Figure 3.7 MATLAB Simulink representation of SMIB system with no PSS installed

3.3.2 Single machine infinite bus system eigenvalues and torques

Table 3.1 shows the Eigenvalues of the system and the associated damping ratio:

Table 3.1 The Eigenvalues and Damping Ratios of the System with no PSS Installed

Eigenvalue	Damping Ratio
-1.1294 + 2.8856i	0.3645
-1.1294 - 2.8856i	0.3645
0.016 + 6.2i	-0.002
0.016 - 6.2i	-0.002

As indicated in Table 3.1, the single machine infinite bus exhibits an unstable oscillatory mode with a frequency of 6.2 rad/sec (1 Hz). Figure 3.8 shows the speed deviation of the single machine infinite bus after being subjected to a disturbance (0.05 increase in mechanical torque).

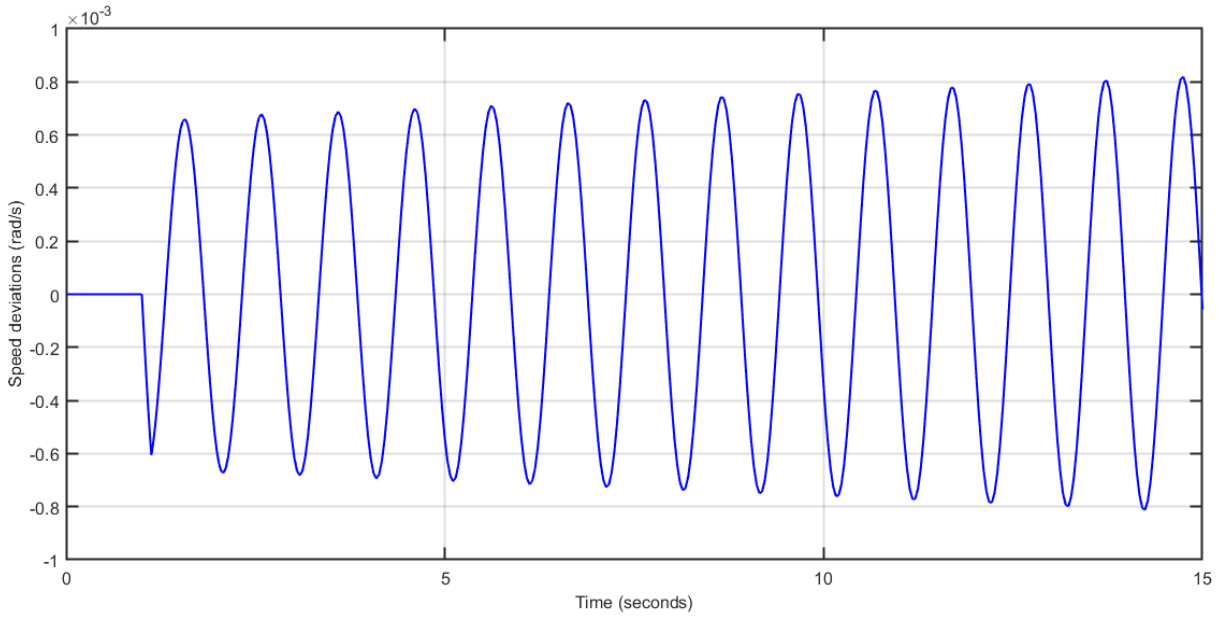

Figure 3.8 Speed deviation due to increase in mechanical torque with no PSS installed

The electrical torques of the single machine infinite bus are obtained by substituting s = $j\omega$ in Equations 3.22 and 3.23. The reader may refer to Appendix A, which states the matrices needed to calculate the electrical torques. Figures 3.9 and 3.10 show the developed torques from both paths.

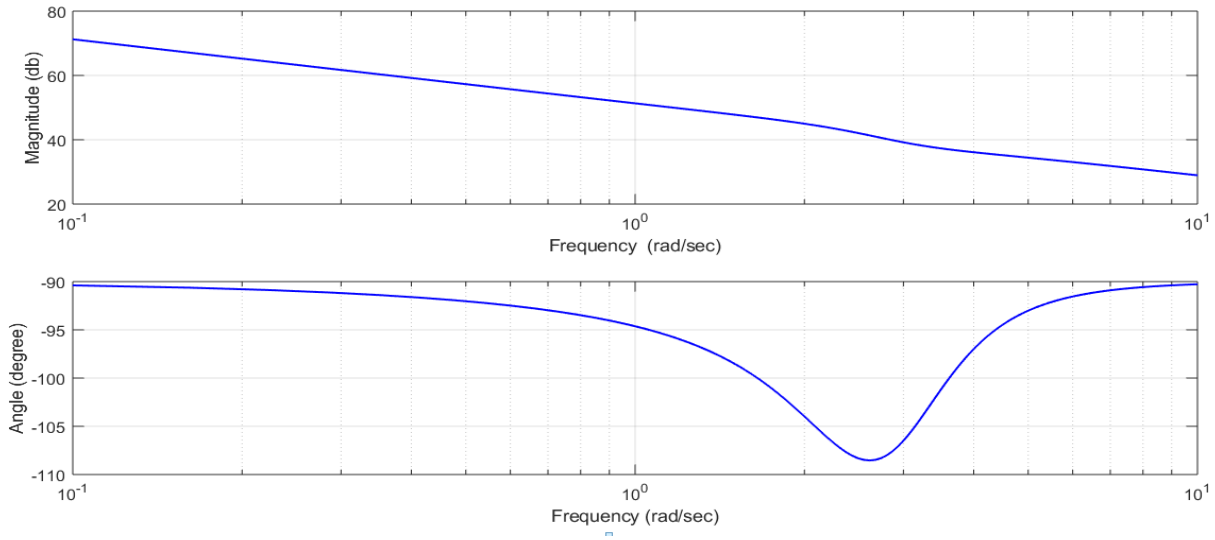

Figure 3.9 Electrical torque from speed deviation $\Delta\omega$

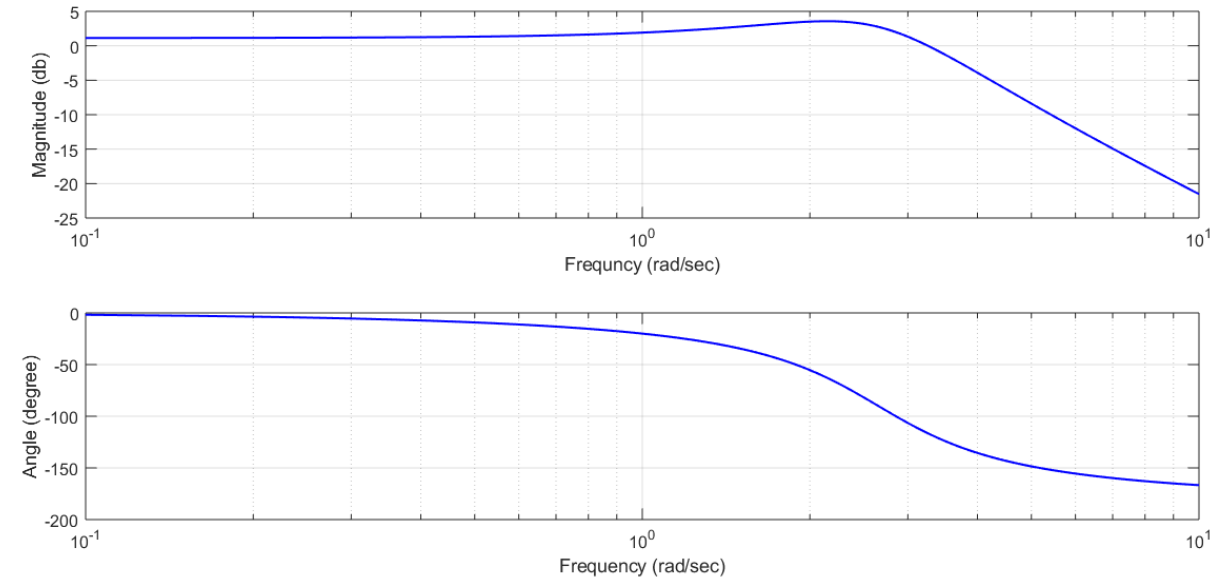

Figure 3.10 Electrical torque from reference voltage input Δv_{ref}

The torques in Figures 3.9 and 3.10 can also be obtained from the Simulink diagram by plotting the bode diagram of the transfer function between $\frac{\Delta P_e}{\Delta\omega}, and\ \frac{\Delta P_e}{\Delta v_{ref}}$.

Figure 3.9 shows that the torque developed has a large imaginary component that does not contribute to damping. Furthermore, the damping torque which constitutes the real part of this torque has a negative or zero value given by the cosine of the angle which ranges between -90 and -110 degrees, therefore is destabilizing. This result is consistent with the eigenvalues calculated in Table 3.1 which indicate unstable electromechanical mode

3.4 Novel Concept to Tune Power System Stabilizer

The main objective of the power system stabilizer is to provide positive damping at frequencies of system oscillations (0.1- 2 Hz). Figure 3.11 shows the torque developed at frequency 1 Hz. The damping torque component of this torque which is the real part is negative, thus, it does not contribute to damping.

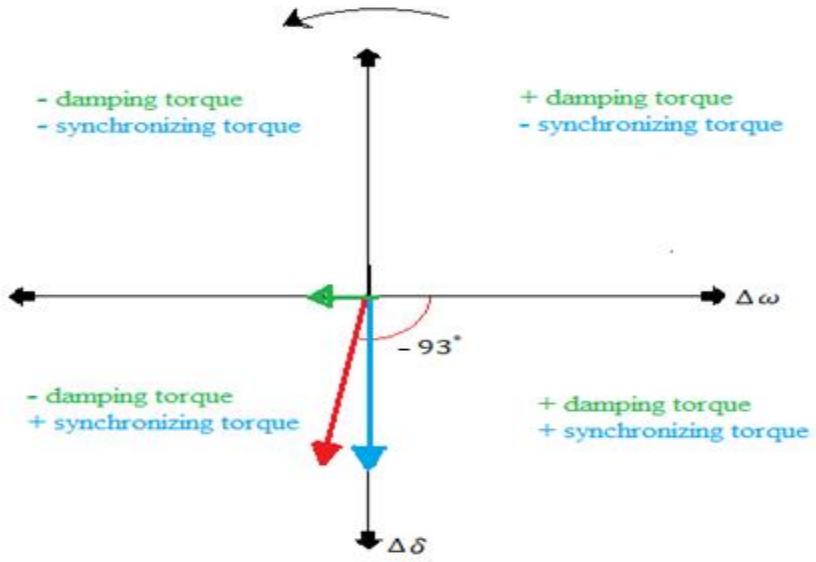

Figure 3.11 Synchronizing and damping torques developed at frequency = 1 Hz or 6.135 rad/sec

The following criteria can be used to tune the power system stabilizer such that the torque developed at this frequency is in-phase with speed deviation:

Referring to Figure 2.5, the perturbations in the voltage reference input of the exciter can be expressed as a function of the power system stabilizer with an input $\Delta\omega$ as:

$$\Delta v_{ref} = Gpss(s).\Delta\omega \qquad 3.48$$

Where $Gpss(s)$ is the transfer function of the power system stabilizer.

Hence, Equation 3.21 that relates the generator electrical torques with the speed deviations and the exciter input becomes:

$$\Delta T_e = K(s)\Delta\omega + L(s).Gpss(s).\Delta\omega \qquad 3.49$$

The above equation directly relates the power system stabilizer to the electrical torque developed at each frequency ΔT_e. Thus, one way to provide positive damping torque to the poorly damped modes is to set the value of ΔT_e equals to $abs(K(j\omega))$ as shown in Figure 3.12. In other words, the PSS is tuned to correct the out of phase electrical torque. Mathematically:

$$abs(K(j\omega)) = K(j\omega) + L(j\omega).Gpss(j\omega) \qquad 3.50$$

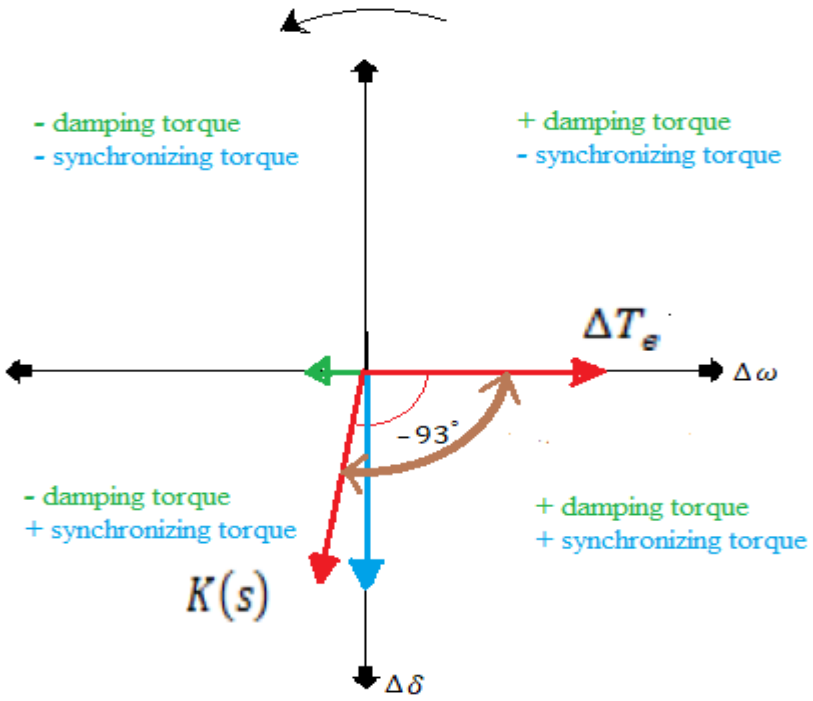

Figure 3.12 Electrical torque phase rotation due to the PSS action

Solving for $Gpss(j\omega)$:

$$Gpss(j\omega) = \frac{abs(K(j\omega)) - K(j\omega)}{L(j\omega).} \qquad 3.51$$

Equation 3.51 gives the magnitude and the phase angle of the power system stabilizer function at a frequency equal to $j\omega$. As a result, these values can be used to calculate the PSS parameters as follows:

A PSS with identical n stages, and 10:1 ratio between the lead and the lag compensator time constants can be described by the following transfer function:

$$G_{PSS}(j\omega) = Kss \times (\frac{1 + j\omega T_1}{1 + 0.1j\omega T_1})^n \qquad 3.52$$

The magnitude and the phase angle of this transfer function shall be described by mag, and ang for the rest of this discussion, can be written as:

$$mag(G_{PSS}(j\omega)) = Kss \times \left(\frac{1 + (\omega T_1)^2}{1 + (0.1j\omega T_1)^2}\right)^{n/2} \quad 3.53$$

$$ang(G_{PSS}(j\omega)) = n * (\tan^{-1}(1 + \omega T_1) - \tan^{-1}(1 + 0.1j\omega T_1)) \quad 3.54$$

Equations 3.53 and 3.54 can be solved for Kss and T_1, the PSS gain and time constant, respectively. These values give the magnitude and the phase angle obtained by Equation 3.50. Figure 3.13 shows the required power system stabilizer function $G_{PSS}(j\omega)$ for the single machine infinite bus.

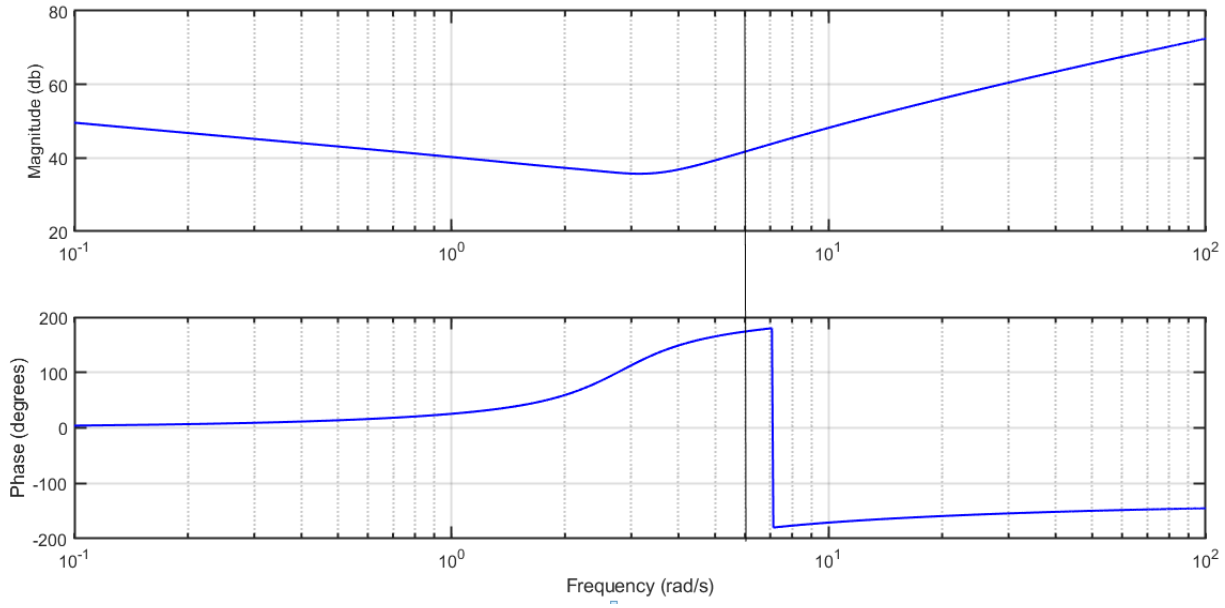

Figure 3.13 Required transfer function of the power system stabilizer

The PSS is designed to provide damping for the electromechanical mode, therefore Equation 3.52 and 3.53 were solved at electromechanical mode frequency, i.e. $j\omega$ = 6.135 rad/sec or 1 Hz. Due to the phase shift requirements, three stages were used to provide the sufficient phase advance. The values of the gain and time constant T1 are found to be as follows:

PSS gain (Kss) = 26 p.u., the time constant T1 = 0.3054 sec. The designed PSS bode diagram is shown in Figure 3.14.

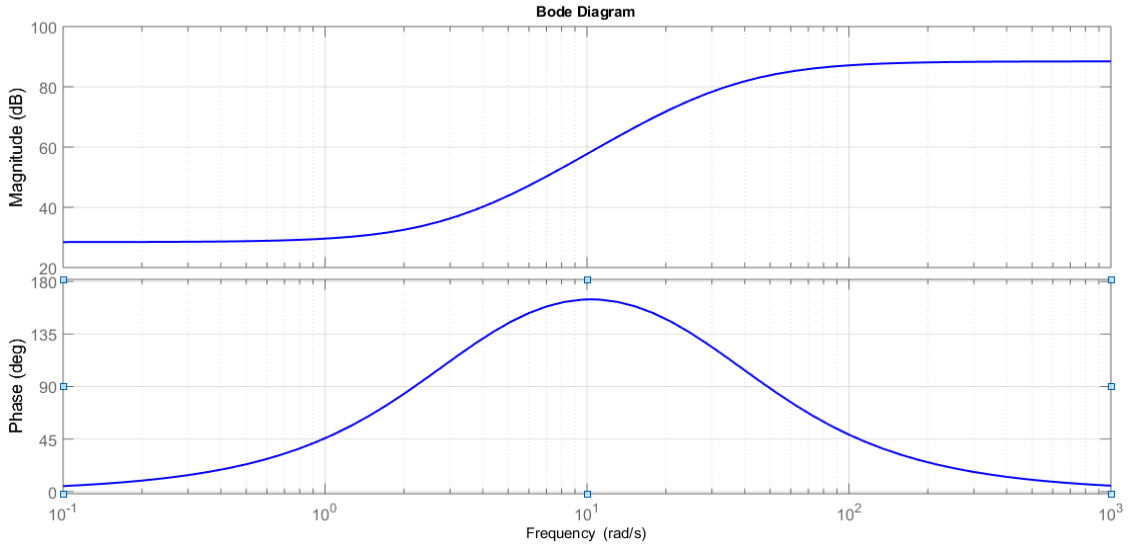

Figure 3.14 Bode diagram of the designed PSS

3.5 Implementation of the Designed PSS on the SMIB Model

This section discusses the implementation of the designed PSS, and the assessment of its performance. Figure 3.15 shows the modified SMIB model after adding the designed PSS. In this model, speed deviations $\Delta\omega$ is defined as an input linearization point and electrical power P_e as an output linearization point. The linearized model is used to plot the zero-pole map, bode diagram to reflect the effect of the power system stabilizer application.

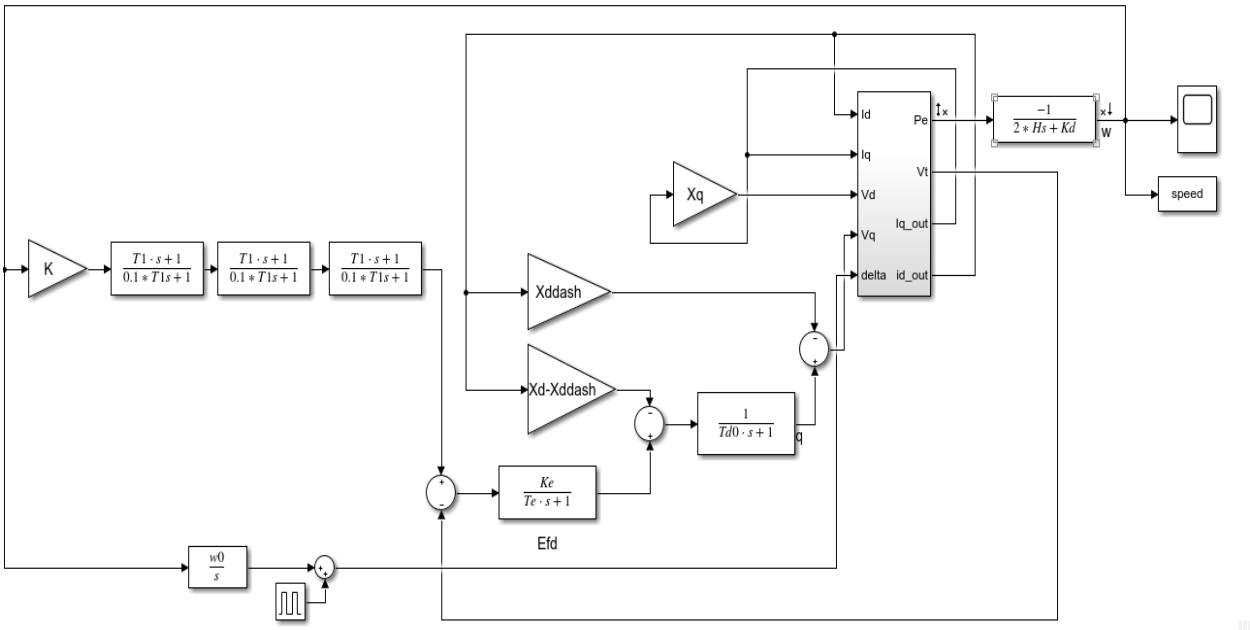

Figure 3.15 Simulink representation of SMIB system with the PSS installed

Table 3.2 shows the electromechanical mode, damping ratio. Figures 3.16 and 3.17 present the pole zero-map, bode diagram before and after applying the PSS, respectively.

Table 3.2 The Eigenvalues and Damping Ratios Before and After Applying the PSS

	Eigenvalue	Damping Ratio
Before applying the PSS	0.016 + 6.2i	-0.02
After applying the PSS	-3.986 + 3.967i	0.709

Table 3.2 shows that the PSS succeeded to provide the sufficient damping torque to the electromechanical mode from being negatively damped to having a damping ratio of 70%.

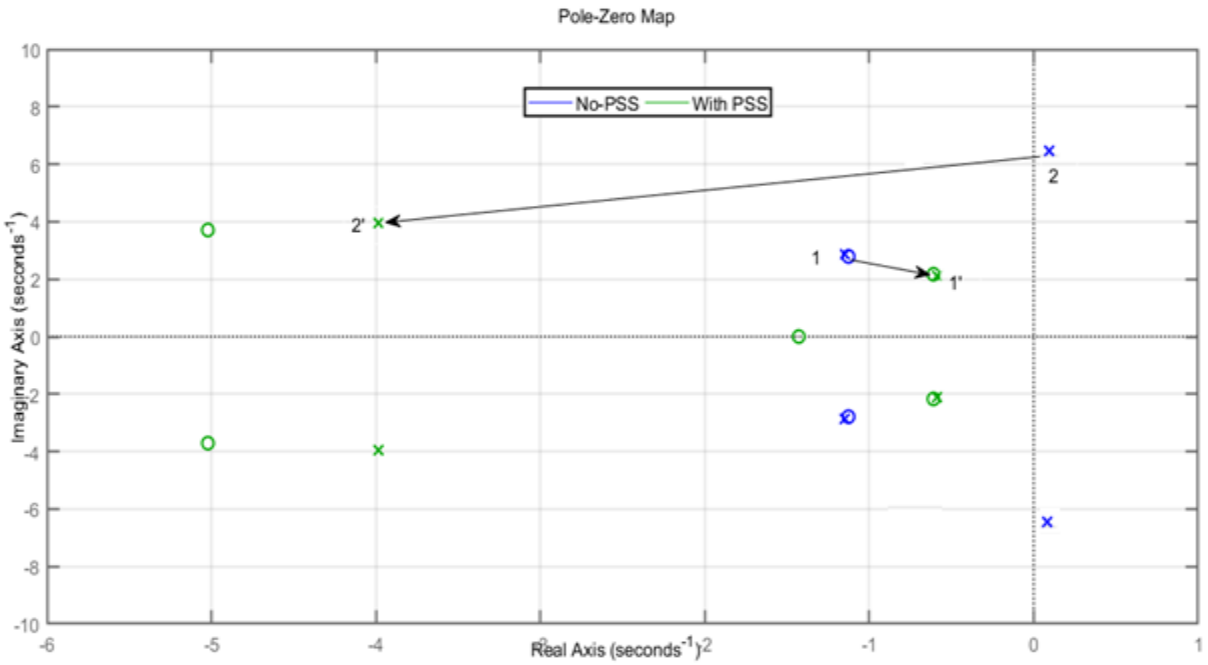

Figure 3.16 Pole zero map of SMIB before and after applying the PSS

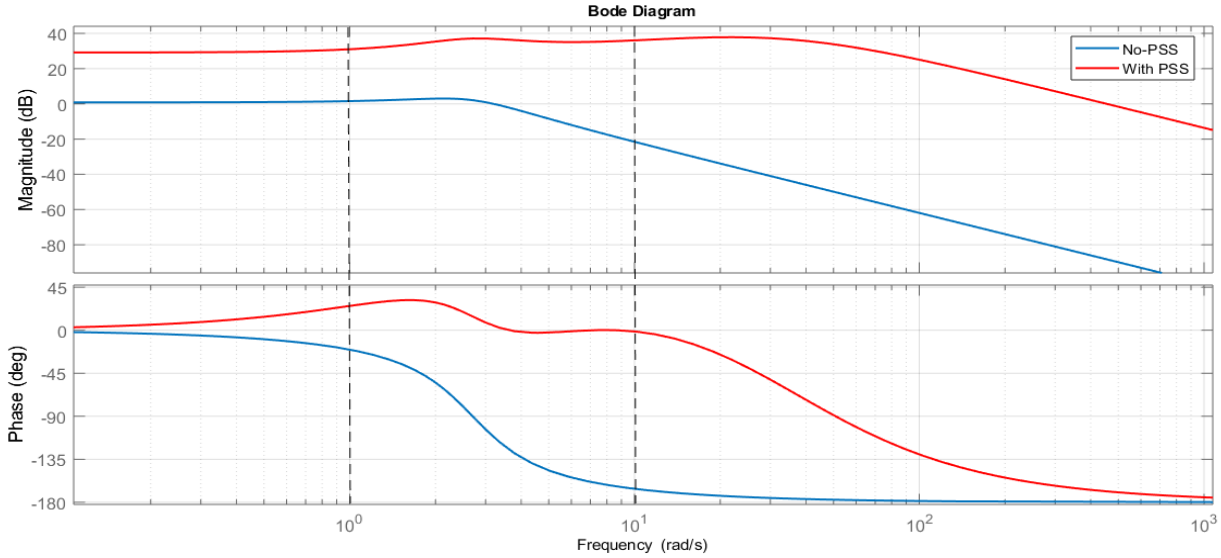

Figure 3.17 Bode diagram of SMIB before and after applying the PSS

The pole zero map shown in Figure 3.14 indicates an improvement in the electromechanical mode damping by 70%. The designed PSS was able to relocate the

electromechanical mode from location 2 to location 2'. On the other hand, the electrical (exciter) mode experienced slight degradation.

Figure 3.15 illustrates how the designed PSS was able to correct not only the phase of the electromechanical mode from low, and negative electrical torque to high, and positive torque, but also, for the marked region (between 1-10 rad/s i.e. 0.1-2 Hz) which is the region of interest. Figure 3.18 shows the speed response due to a positive change in mechanical torque by 0.05.

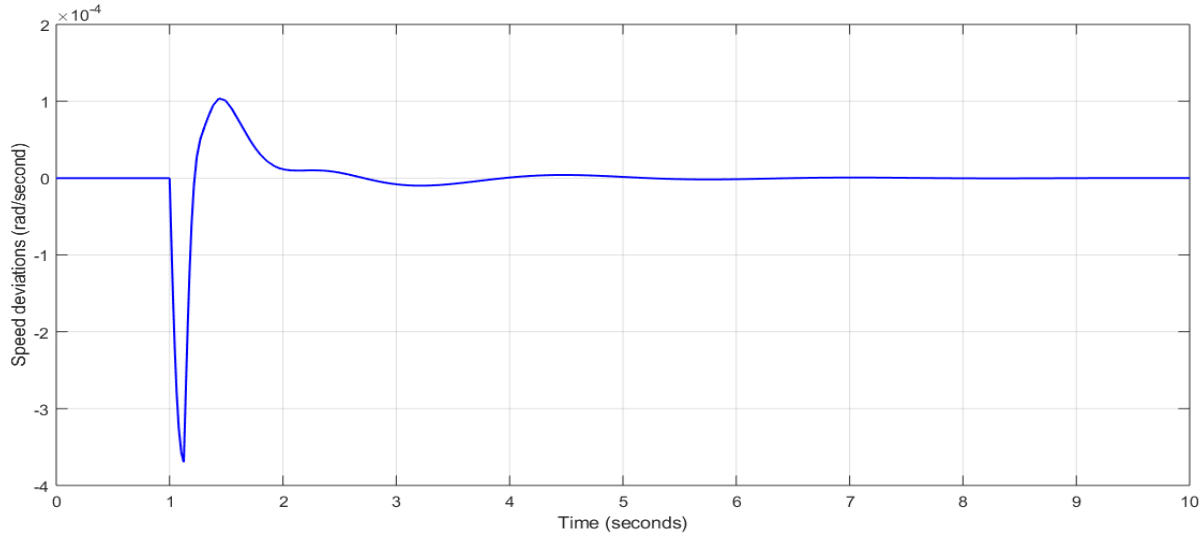

Figure 3.18 Speed deviation due to increase in mechanical torque with the PSS installed

3.5.1 Robustness assessment

In this section, the robustness of the proposed PSS is examined. Different loading conditions are presented in Table 3.3. These loading conditions affect the terminal voltage, rotor angle, and the power factor, therefore, change the dynamic response of the synchronous machine.

Table 3.3 Loading Conditions Cases

Case	P (p.u)	Q (p.u)
A (base case)	0.9	0.3
B	1.2	0.45
C	0.9	0.2
D	0.45	0.077

Figure 3.19 shows the pole zero map of each case. The designed PSS provided good damping for the electromechanical modes at each case. Note that the exciter mode was affected considerably in case B as it represents high loading conditions.

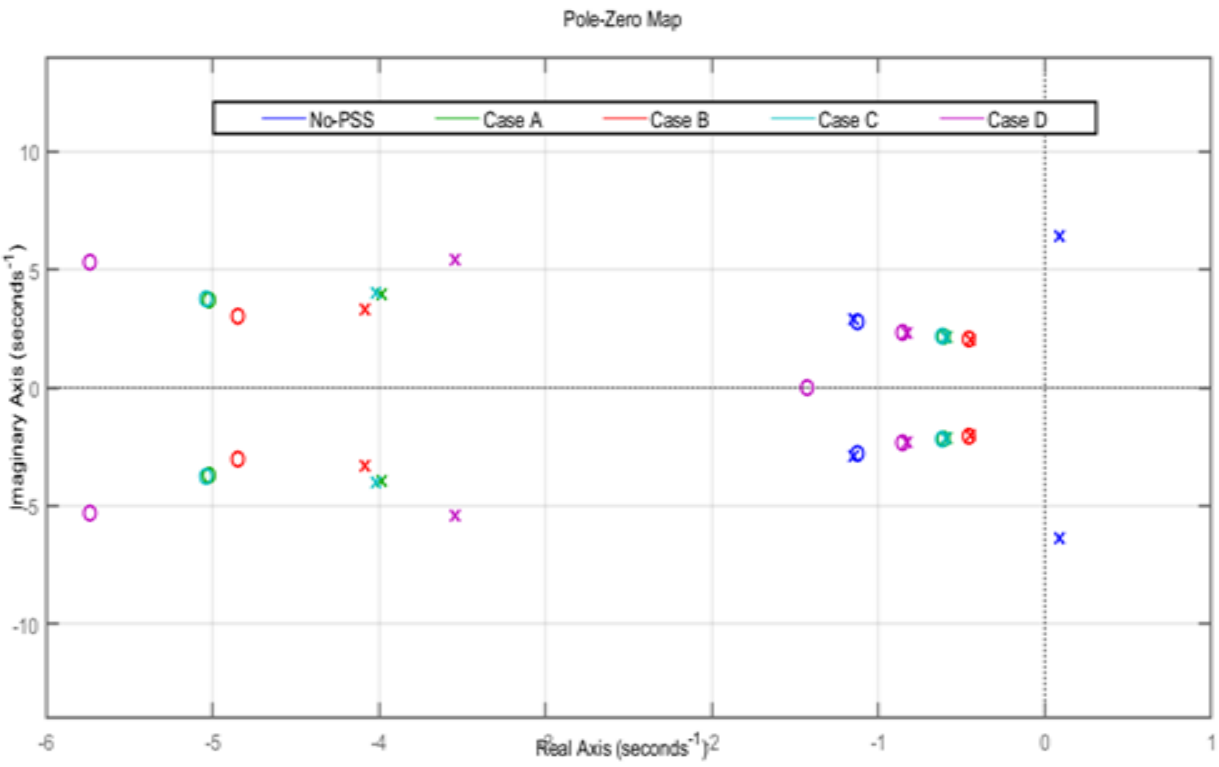

Figure 3.19 Pole zero map of each case

3.6 The Procedure of Tuning the Power System Stabilizer Using Out of Phase Torque Correction

The proposed method can be used to tune the power system stabilizer in a multimachine environment. Note that for multimachine system with n generators, Equation 3.49 becomes:

$$\begin{bmatrix} \Delta T_{e1} \\ \vdots \\ \Delta T_{en} \end{bmatrix} = K(s)\begin{bmatrix} \Delta\omega_1 \\ \vdots \\ \Delta\omega_n \end{bmatrix} + L(s).Gpss(s).\begin{bmatrix} \Delta\omega_1 \\ \vdots \\ \Delta\omega_n \end{bmatrix} \quad 3.55$$

Where:

$K(s)\ is\ n \times n\ matrix.$

$L(s)\ is\ n \times n\ matrix.$

$Gpss(s)\ is\ n \times n\ diagonal\ matrix.$

The following steps are performed to tune the power system stabilizer:

1. Build the system state matrix as explained in section 3.3.1. Find the system eigenvalues by solving Equation 3.19.
2. Identify poorly damped eigenvalues (modes).
3. Use Equations 3.22 and 3.23 to calculate the electrical torques at the least damped mode frequency identified in step 2.
4. The diagonal elements of the matrix obtained by solving Equation 3.51 give the magnitude and phase shift required by the power system stabilizer.
5. Find the power system stabilizer parameters by solving Equations 3.54 and 3.55, simultaneously.

CHAPTER 4

RESULTS AND DISCUSSION

The following chapter demonstrates the implementation of the proposed power system stabilizer on several test systems. The performance of the PSS was compared against designs that were found in literature [2], [12], and [13].

4.1 Two-Area Four-Machine system

This system consists of two areas, each of them has identical generation composed of two 900MVA /20KV units. The two areas are linked by a high voltage transmission double line rated at 230 KV. The complete description of the data is listed in Appendix B. Figure 4.1 shows the single line diagram of the system.

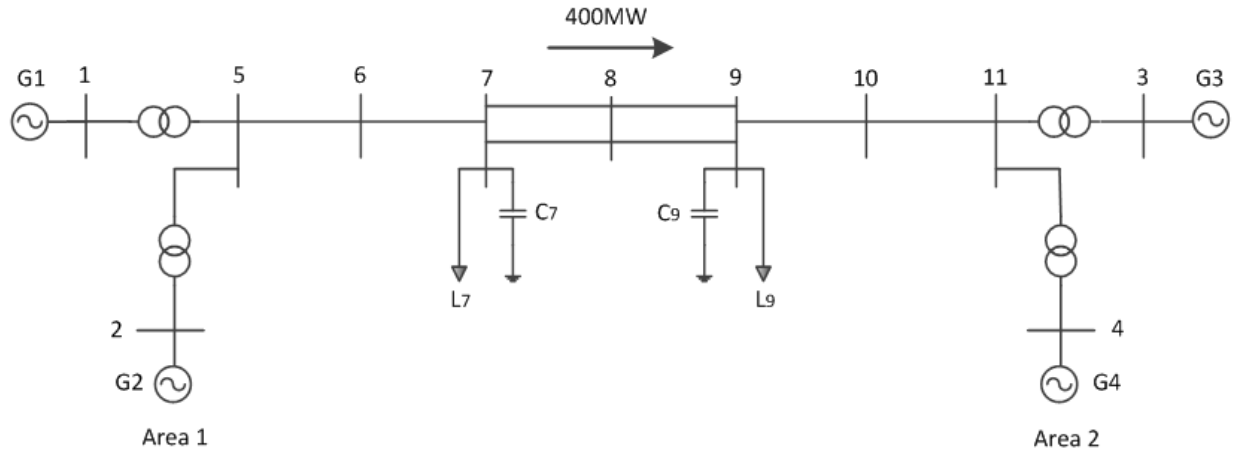

Figure 4.1 Single line diagram of the two-area four-machine system

4.1.1 Eigenvalues and electrical torques analysis

A Simulink model of the system is built by the MathWorks, Inc. team. The model studies the performance of different types of power system stabilizers on damping interarea oscillations, specifically, a conventional Delta-Omega PSS that follows design criteria proposed by P. Kundur, Multi-Band PSS, and a conventional acceleration power PSS.

With no PSS applied, the system experiences undamped oscillatory modes when subjected to a disturbance. Figures 4.2 and 4.3 show the resulting instability.

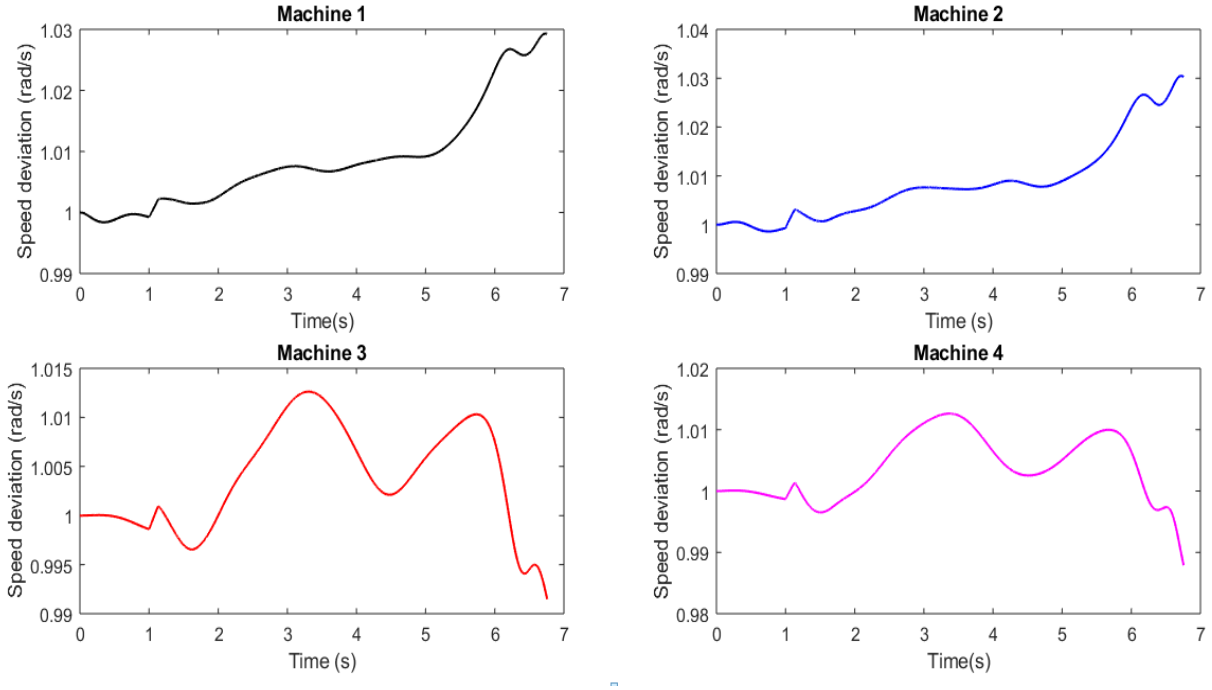

Figure 4.2 Machines speed deviations for a fault on the tie-line for 7 cycles

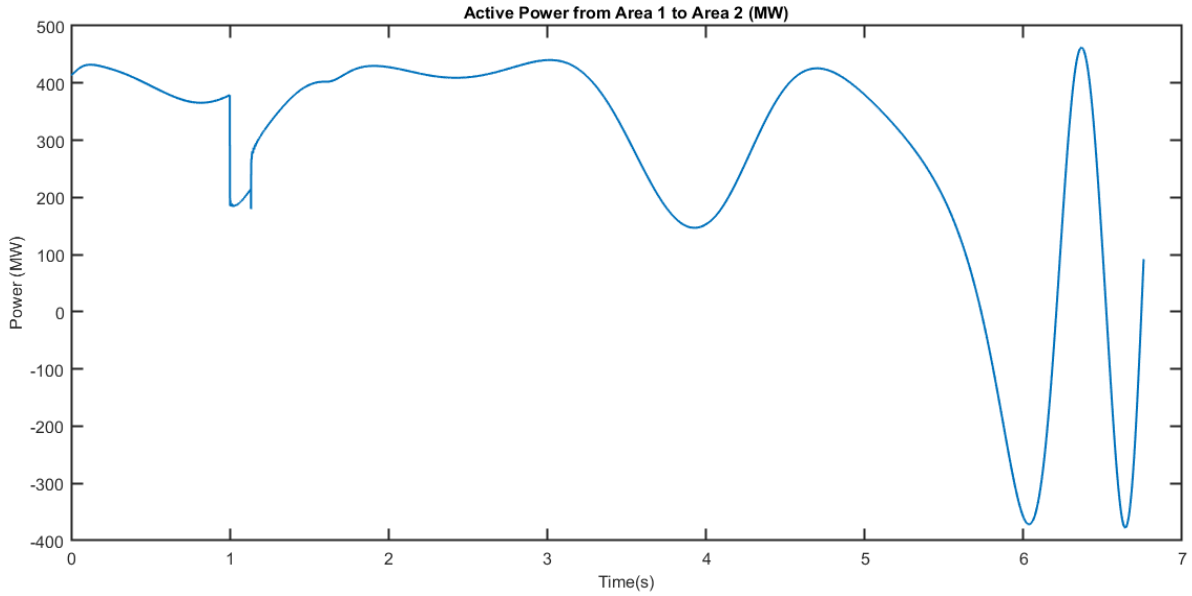

Figure 4.3 Power transferred through the tie line for a fault on the tie-line for 7 cycles

Figure 4.2 presents the speed deviations of the four machines as a result of a fault on the tie line. Loss of synchronism occurred as the two areas start to oscillate against each other in a coherent manner (Machine 1 & 2 oscillate against Machine 3 & 4).

Figure 4.3 illustrates the power transferred from area 1 to area 2. The tie line experiences severe power swings resulting from the machines swinging against each other.

MATLAB Control design feature (Linear analysis) was used to plot the model pole zero map shown in Figure 4.4. The system has one unstable mode at 4 rad/s and two poorly damped modes at 7 rad/s and 7.26 rad/s.

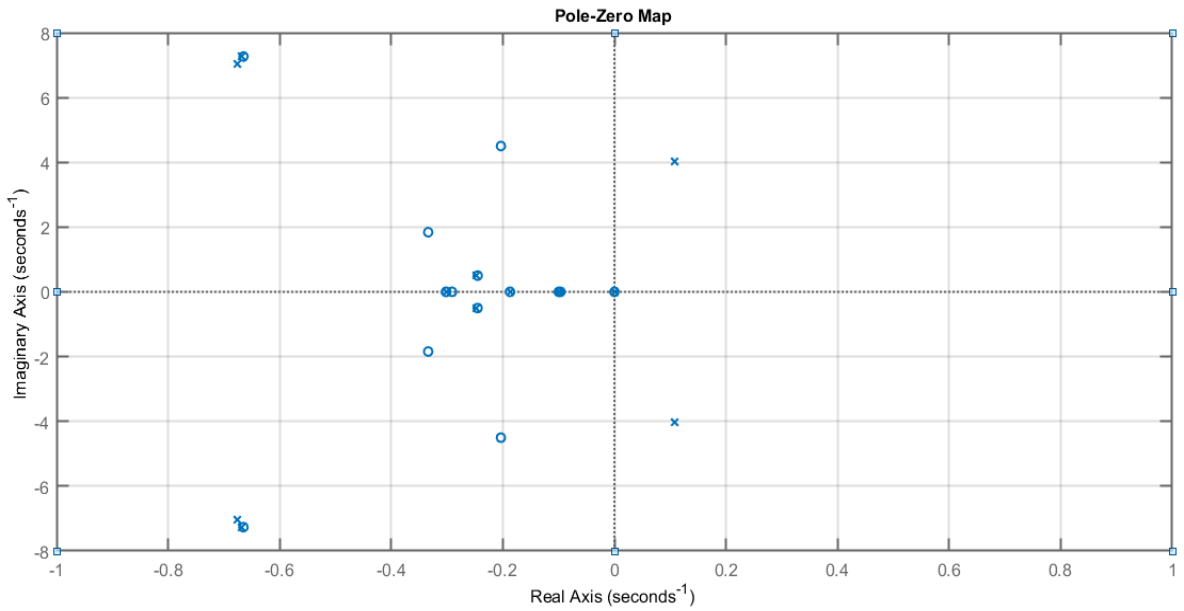

Figure 4.4 Pole zero map of the system

A separate MATLAB code was written to assess the small signal stability of the system. Table 4.1 compares the eigenvalues and their associated damping ratio resulting from the MATLAB script and Simulink model.

Table 4.1 Eigenvalues and Damping Ratios Obtained from Both Models

MATLAB Script		Simulink Model		
Mode	Damping Ratio (%)	Mode	Damping Ratio (%)	Area
0.030±3.93i	-0. 7	0.108±4i	-2.68	Interarea mode
-0.342±6.09i	5.6	-0.67±7.05i	9.5	Local mode(Area 1)
-0.366±6.30i	5.7	-0.677±7.26i	9.2	Local mode (Area 2)

MATLAB script modes were slightly different than those obtained from the Simulink model. This is because the script uses a simplified first order model of the synchronous machine while the Simulink uses a detailed nonlinear model. Yet, both models show unstable interarea mode and two poorly damped local modes.

Equation 3.21 was used to calculate the electrical torque matrix developed at each machine at the frequency of the least damped mode i.e. 3.93 rad/s. It was found to be as follows:

$$\begin{bmatrix} 6.6-565.5j & -10.8+477.1j & -1.1+476.5j & 7.4+332.5j \\ -64.7+426.2j & 16.7-657.84j & 21.9+120.2j & 28.96+107.3j \\ 0.75+134.4j & 1.5+126.8j & 20-672.7j & -11.2+396.5j \\ -8+145j & -9.2+148.1j & -42.7+411.6j & 76.5-713j \end{bmatrix}$$

Note that each row gives the electrical torque developed at each machine for all speed components. These values indicate large imaginary components and comparatively low real components. In other words, the damping torque developed at each machine is not sufficient to establish good damping characteristics for the electromechanical modes.

4.1.2 Power system stabilizer tuning

The procedure described in Section 3.6 was used to tune the two parameters of the four power system stabilizers installed in each machine. Table 4.2 summarizes the values of the time constant and the overall gain of each machine.

Table 4.2 Tuned PSS Parameters

Machine No	Gain (p.u)	Time constant (s)
1	39	0.1435
2	34.28	0.1224
3	37.12	0.1539
4	26.82	0.1428

The new modes of system are provided in Table 4.3 below:

Table 4.3 System Modes After Applying the Designed PSS

Mode	Damping Ratio (%)	Area
-1.07±3.38i	31	Interarea mode
-2.05±4.23i	43	Local mode (Area 1)
-3.28±2.95i	74	Local mode (Area 2)

Table 4.3 shows the improvement in the interarea mode from being unstable to having a damping ratio of 30%. The damping of the local modes has improved as well.

The developed torques after applying the designed can be calculated using Equation 3.49. The torques developed at the unstable electromechanical mode were found to be as follows:

$$\begin{bmatrix} 807+18.4j & -410.7+375j & 5.22+67.8j & 56.57+78.7j \\ -646+113j & 890-165.7j & -10.5+123.8j & 47.6+147.4j \\ -32.6+111.7j & 13.5+131.9j & 819+5.1j & -293+310j \\ -66.7+101.7j & -58.5+136.4j & -590+104.5j & 825+149j \end{bmatrix}$$

It worth mentioning that, the designed PSS contributes a large positive component to the diagonal elements. The contribution to the off-diagonal elements is not zero since the PSS utilizes local speed only.

4.1.3 Performance comparison of two power system stabilizers

In this section, the performance of the designed PSS was compared to the MB-PSS provided by MATLAB Simulink model where the two stabilizers utilizes the same stabilizing signal. Furthermore, MB-PSS outperformed the other two PSS found in the model. Figure 4.5 shows the structure of the MB-PSS compared to the designed PSS.

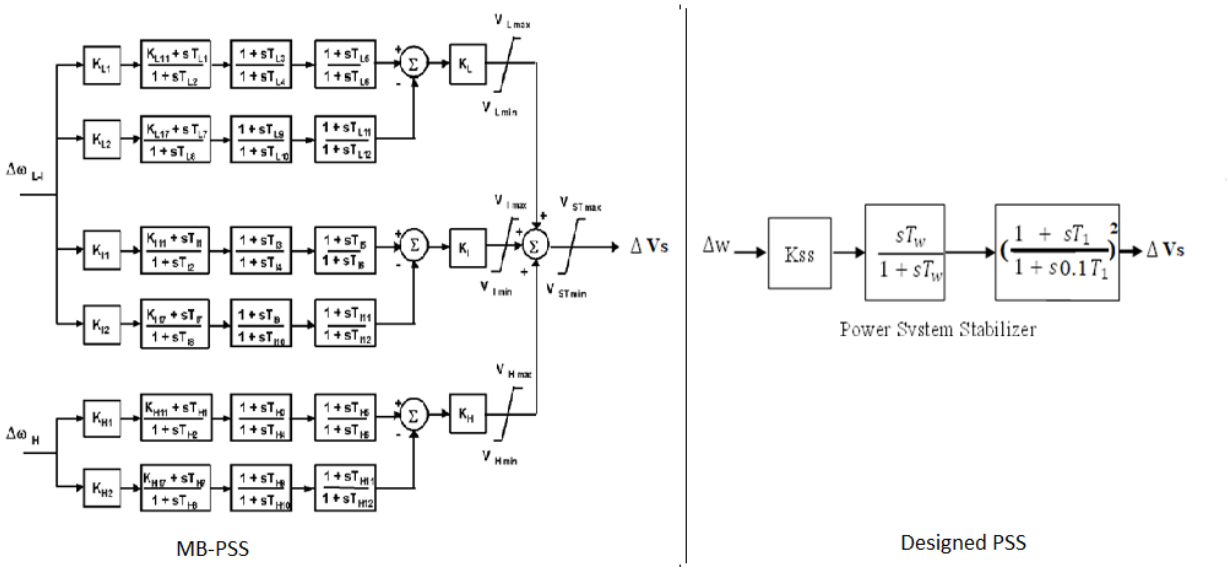

Figure 4.5 Structure of the MB-PSS compared to the designed PSS

For comparison purposes, the bode diagram and the pole zero map of the two PSSs is plotted as shown in Figures 4.6 and 4.7, respectively.

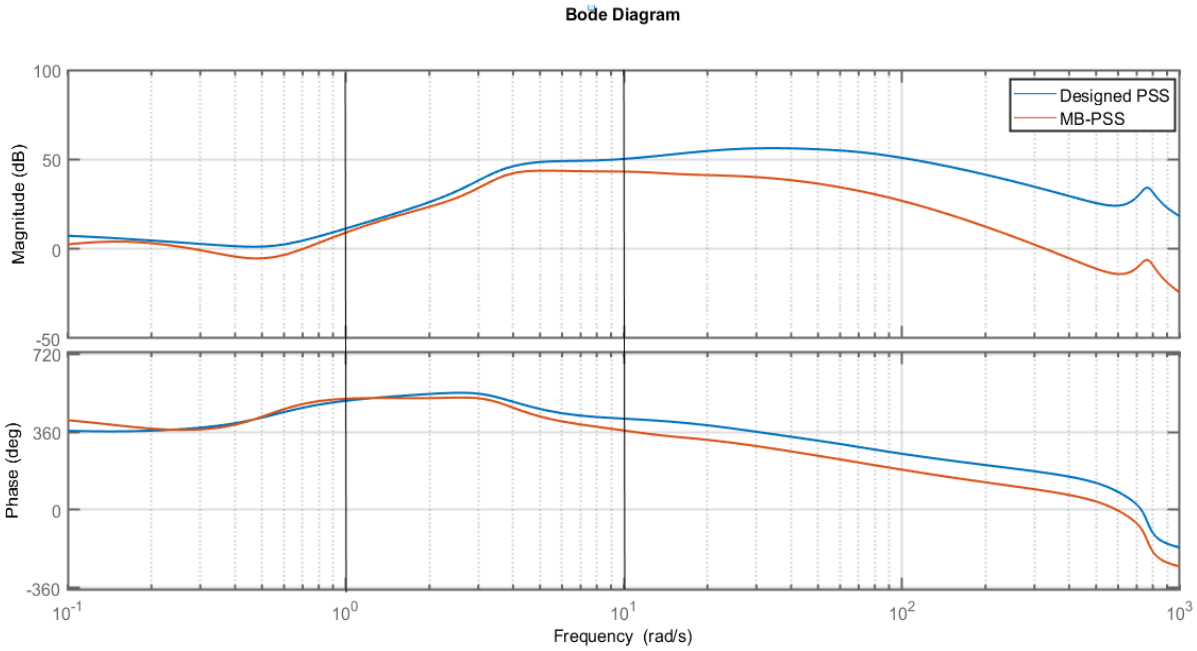

Figure 4.6 Bode diagram of the two stabilizers

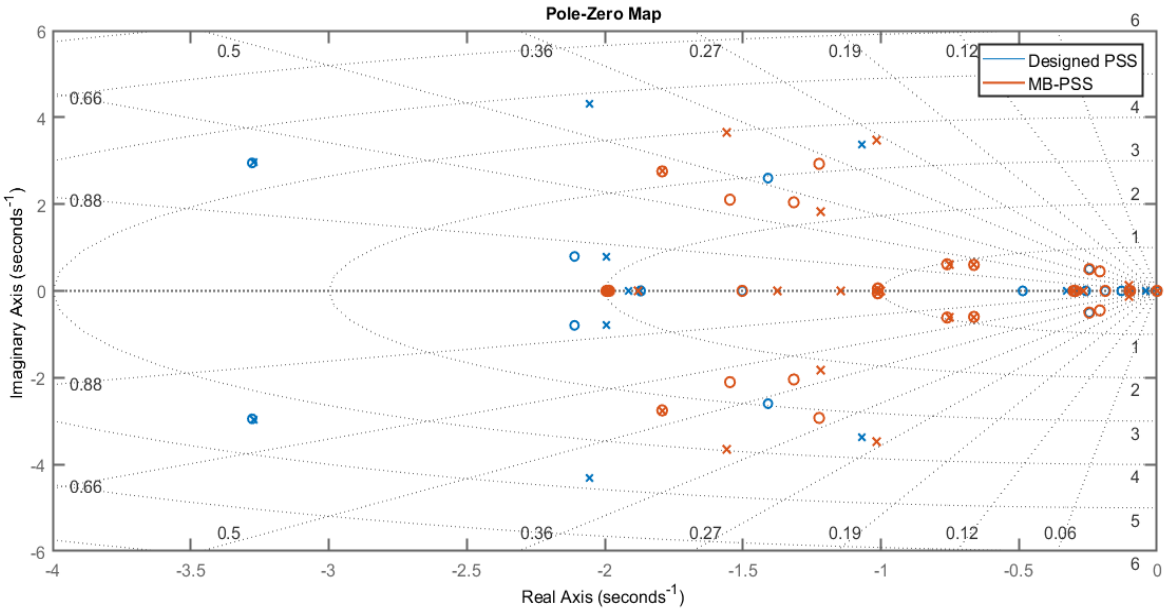

Figure 4.7 Pole zero map of the two stabilizers

The bode diagram shown in Figure 4.6 confirms the superiority of the designed PSS over the MB-PSS. The designed PSS was able to provide better gain/phase characteristics in the region of interest compared the MB-PSS. Moreover, Figure 4.7 shows the pole zero map of the system with both stabilizers installed; again, the designed PSS provided better damping than the MB-PSS by shifting the modes of the system further to the left-hand side.

Time domain simulation performance of both stabilizers was also verified. Figures 4.8 and 4.9 display the machine speed, and the power transferred through the tie line when applying both stabilizers.

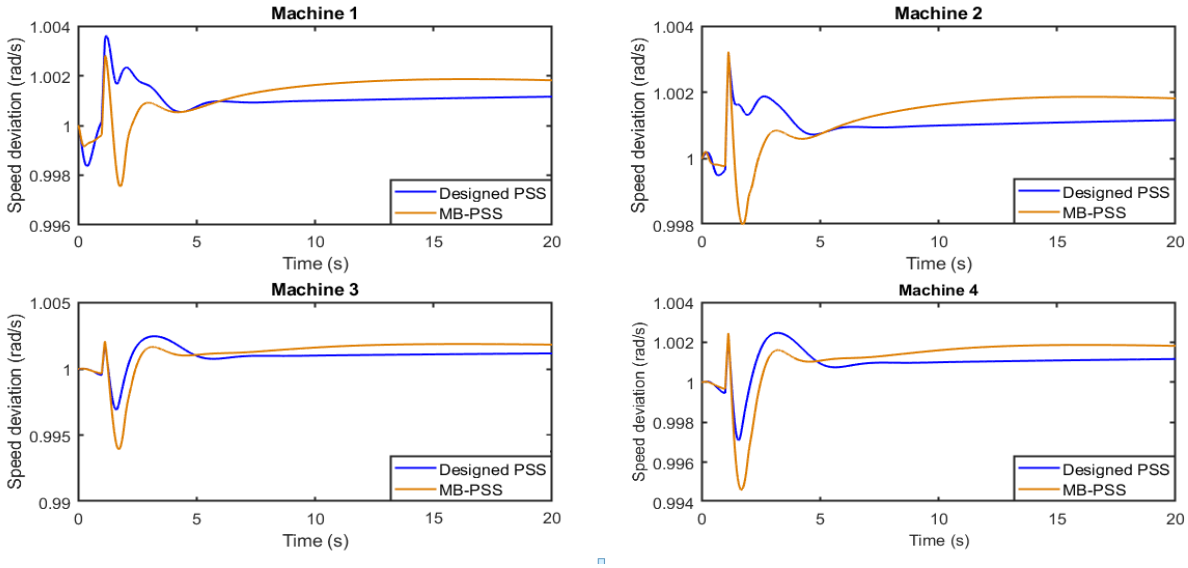

Figure 4.8 Speed deviations of the four machines

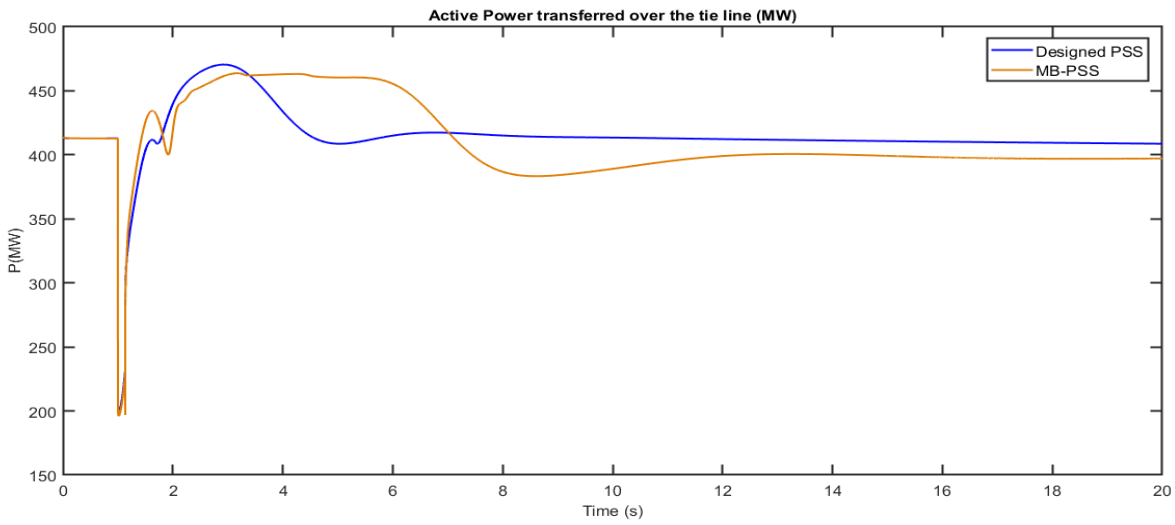

Figure 4.9 Active power transferred over the tie line

Above Figures demonstrate how the designed PSS outperformed the MB-PSS in all aspects of stability. Figure 4.8 shows that the designed PSS have better overshoot characteristics therefore, helping the system to reach an equilibrium point in shorter period. Furthermore, Figure 4.9 demonstrates that the new designed PSS caused disturbance stress on the tie line by diminishing power oscillations.

4.1.4 Robustness assessment

The performance of the proposed PSS was tested at different loading conditions. Under base load conditions the system is operating near the nominal rated capacity, i.e. the machines were 77% loaded.

Load flow analysis was used to find the new operating point of the system. For heavy loading conditions the loads were increased by 11%, the new operating point was found to be 86%. On the other hand, light loading conditions assumes the loads were reduced by 50%. Table 4.4 summarizes the loading conditions of each case.

Table 4.4 Different Loading Conditions Cases

Case	Operating conditions (%)
Base case	77%
Heavy loading case	86%
Light loading case	50%

Figure 4.10 shows the pole zero map of each case with the designed PSS installed. Although the PSS was designed at the base case operating conditions, it provided good damping performance on the extreme conditions as well.

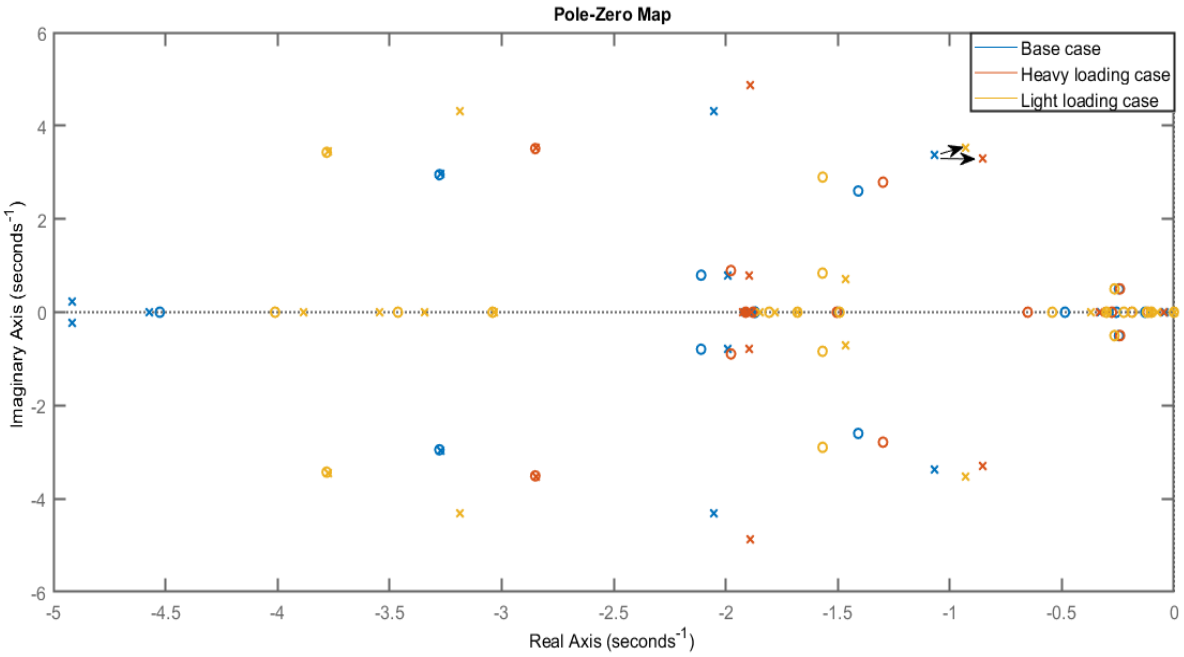

Figure 4.10 Pole zero map of each loading case with the designed PSS installed

4.2 IEEE 9 Bus System

This system consists of three machines and six transmissions lines. The machines are connected to the transmission lines through three generators step up transformers (GSU). Figure 4.11 shows the single line diagram of the 9-bus system. System data are outlined in Appendix C.

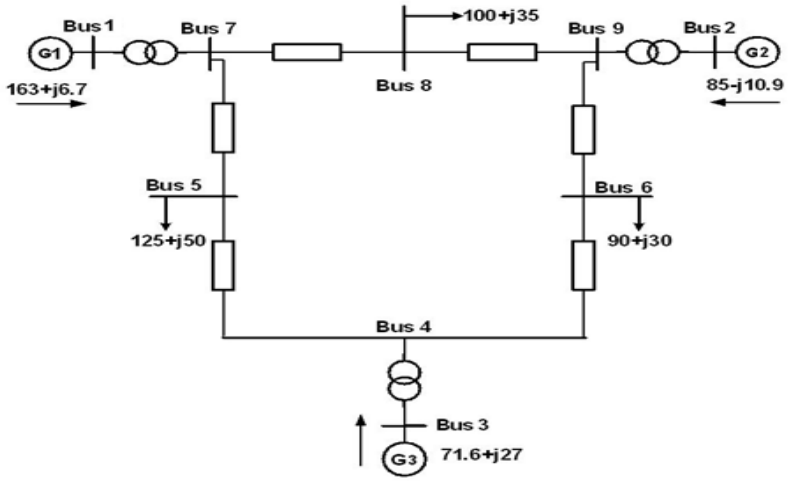

Figure 4.11 Single line diagram of the IEEE 9 bus system

4.2.1 Eigenvalues and electrical torques analysis

Following the same line of analysis shown in section 4.1.1, the small signal response of the system without PSS due to step change in the mechanical power is displayed in Figures 4.12 and 4.13.

Figure 4.12 shows the resulting speed deviations while Figure 4.13 displays the active power generated by each machine. The response indicate oscillatory behavior caused by underdamped modes.

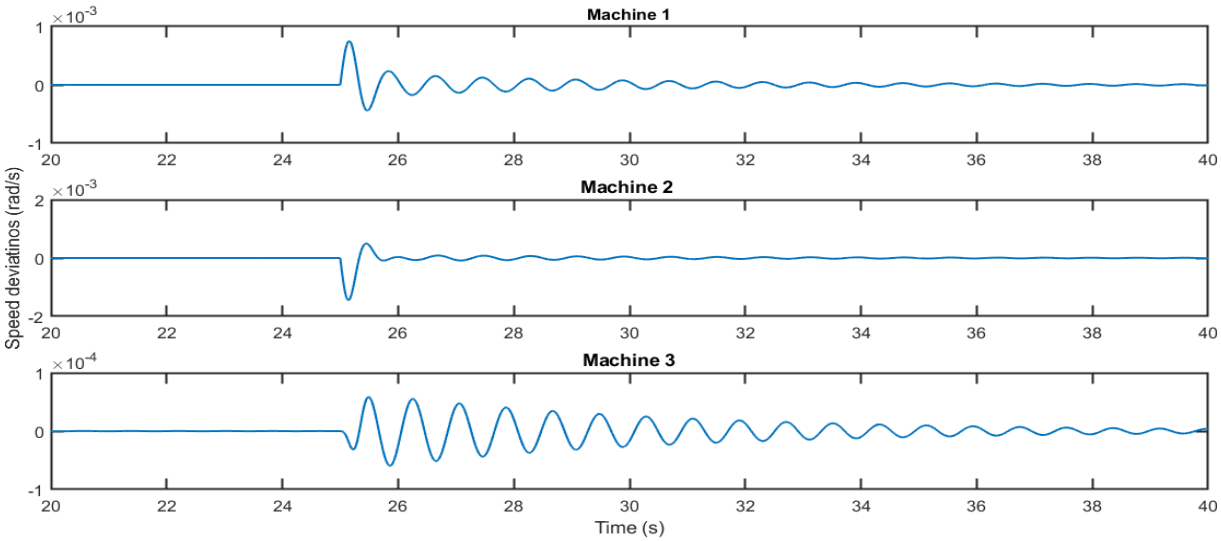

Figure 4.12 Speed deviations due to mechanical step change

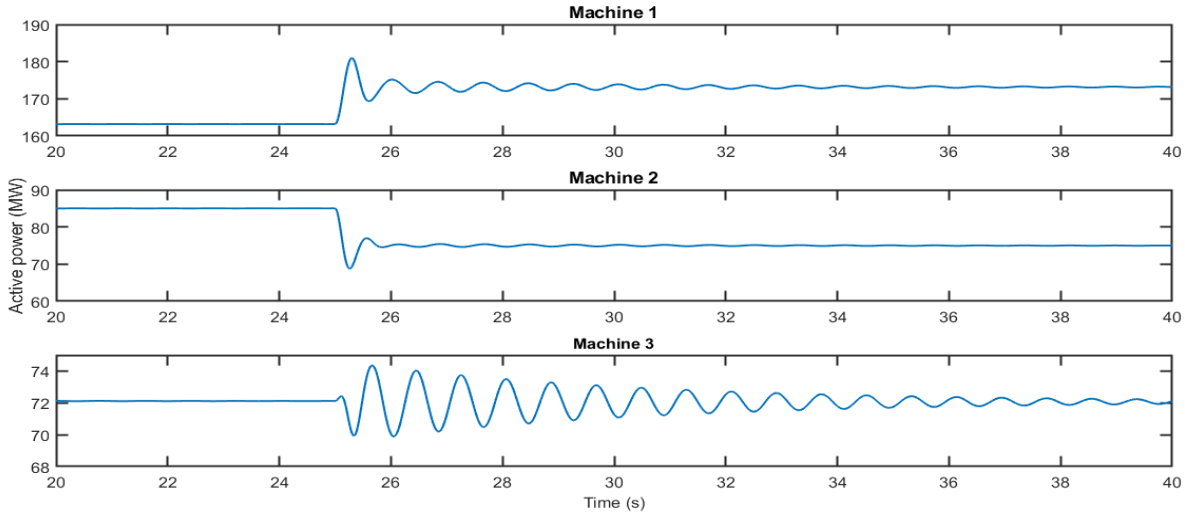

Figure 4.13 Generated active power due to mechanical step changes

A MATLAB script that includes the machines dynamics and the transmission system of the IEEE 9 bus system was used to generate the system modes. Table 4.5 presents the detected electromechanical modes and their associated damping ratios.

Table 4.5 System Modes and Damping Ratio

Mode	Damping Ratio (%)
-7.620±10.022i	60
-2.802±10.588i	25
-0.233±7.795i	3

Equation 3.21 was used to calculate the electrical torques at each machine frequency equals to 7.79 rad/s which is the least damped mode frequency, they were found to be as follows:

$$\begin{bmatrix} 13.2-105.6j & -12.6+32j & -0.7+73.5j \\ -13.2+28.2j & 21-72.7j & -7.8+44.3j \\ -1+78.5j & -3.2+40.5j & 4.3-118.7j \end{bmatrix}$$

The diagonal elements of the matrix above show large imaginary components that do not contribute to damping.

4.2.2 Power system stabilizer tuning

The proposed out of phase torque correction method was used to tune three power system stabilizers installed at each machine. Note that, the PSS parameters to be calculated are the gain, and the time constant. Following the steps of the proposed method. PSS parameters were found to be as shown in Table 4.6 below.

Table 4.6 PSS Calculated Parameters

Machine	Gain (pu)	Time constant (s)
1	15.11	0.0851
2	10.27	0.0927
3	25.82	0.0816

These parameters were then applied to each PSS, the updated modes and damping ratios are presented in Table 4.7.

Table 4.7 Modes and Damping Ratios After Applying the Designed PSSs

Mode	Damping Ratio (%)
-6.09±16.1i	35
-1.42±6.03	23
-3.63±3.81	70

The new torques developed at the electromechanical mode i.e. $j\omega = 7.79\, rad/s$ were found to be as follows:

$$\begin{bmatrix} 152 - 38.27j & -64.7 + 20.9j & -32.9 + 75.9j \\ -81.9 + 12.3j & 107 - 30.6j & -62.8 + 46.4j \\ -39.7 + 56.1j & -17.5 + 29.5j & 155 - 48.3j \end{bmatrix}$$

The PSS contribution to the real component of the electrical torque matrix is obvious. The net damping torque depends on the mode shapes (whether the machines are swinging coherently or against each other), but eigenvalue analysis shows that the net effect is favorable.

4.2.3 Performance of the designed PSS

To assess the performance and the adequacy of the designed PSS, time domain simulation was carried out. Figures 4.14 and 4.15 confirm that the new design has enhanced the overall stability.

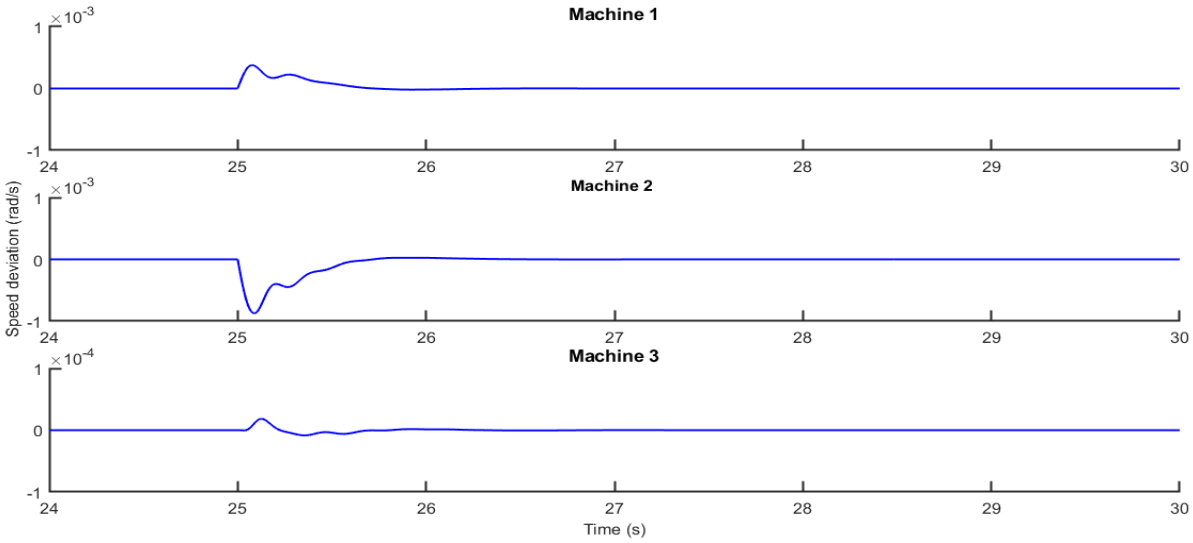

Figure 4.14 Speed deviations due to mechanical step change after installing the PSS

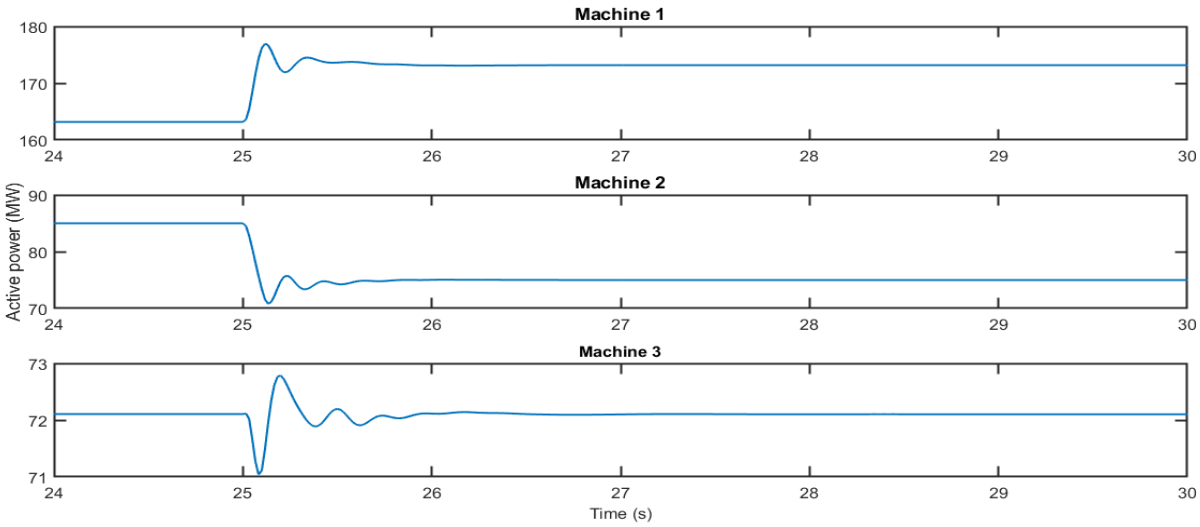

Figure 4.15 Active power due to mechanical step change after installing the PSS

The above response was compared against the response obtained by applying the power system stabilizer proposed by [2]. The design in [2] assumes all the information needed to design a PSS in a multimachine are found locally. As a result, the equivalent voltage of transmission lines emanating from the step-up transformer is used as an infinite bus allowing for design using a SMIB model in a multimachine environment. Figure 4.16 shows the comparison of the two stabilizers.

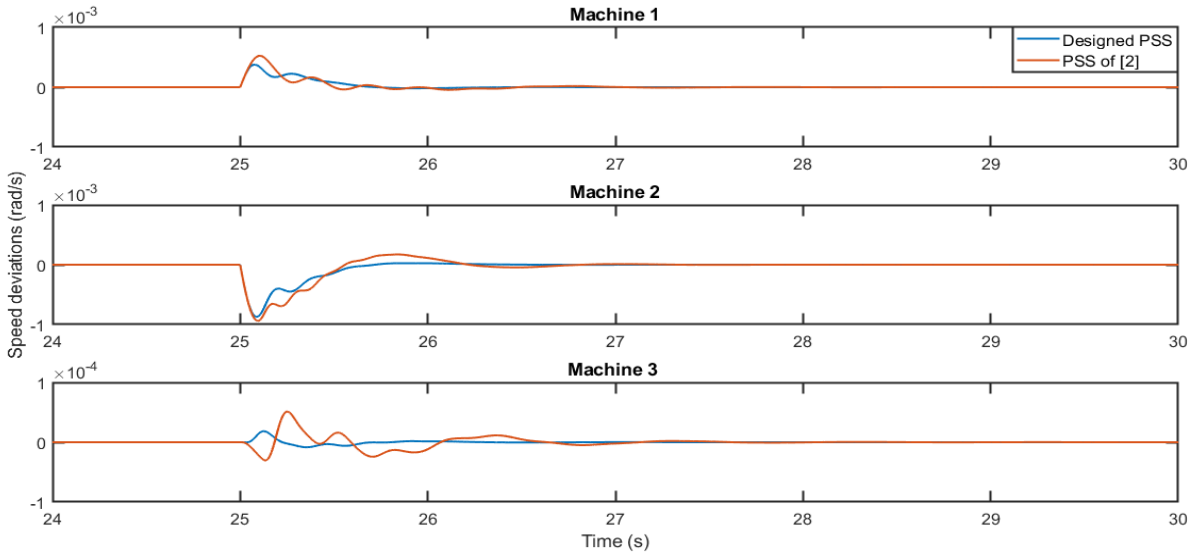

Figure 4.16 Speed deviations resulting from both designs

4.2.4 Robustness analysis

The performance of the proposed PSS was tested at different loading conditions. Heavy loading conditions were obtained from [2]. Light loading was set to be 50% off the base case. The loading conditions are tabulated in Table 4.8.

Table 4.8 Different Loading Conditions of the IEEE 9 Bus System

No.	Base case		Heavy loading [2]		Light	
	P (p.u)	Q (p.u)	P (p.u)	Q (p.u)	P (p.u)	Q (p.u)
Gen 1	1.63	0.07	1.92	0.56	0.82	-0.279
Gen 2	0.85	-0.11	1.28	0.36	0.45	-0.353
Gen 3	0.72	0.27	2.21	1.09	0.33	-0.1355
Load 1	0.9	0.3	1.8	0.6	0.45	0.15
Load 2	1.25	0.5	2	0.8	0.62	0.25
Load 3	1	0.35	1.5	0.6	0.5	0.175

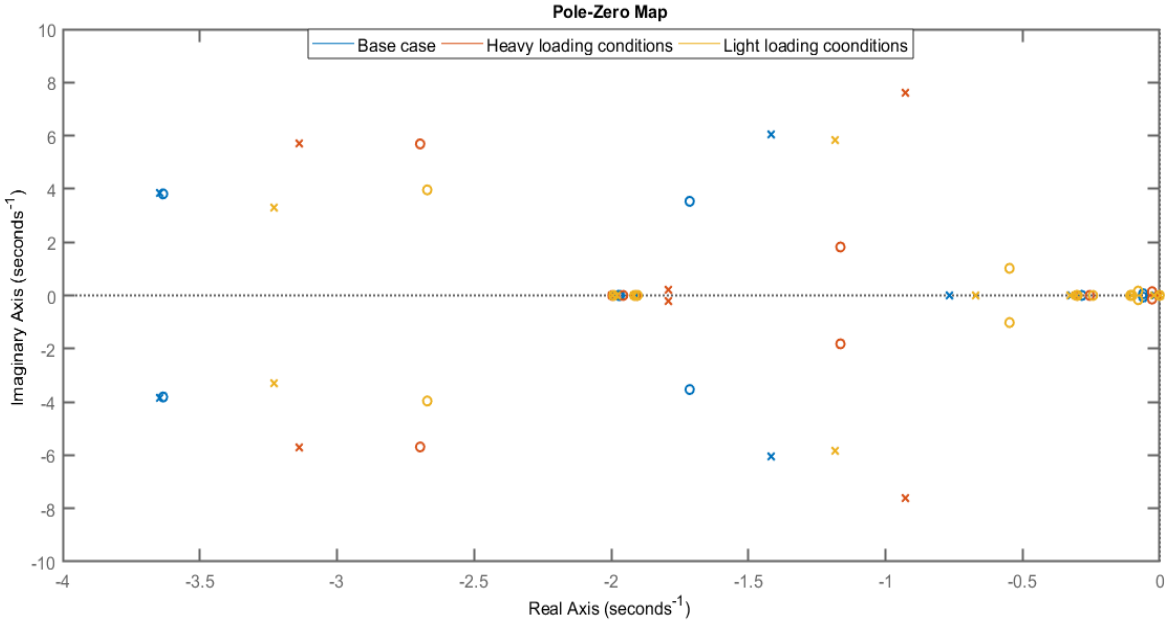

Figure 4.17 Pole zero map of each loading condition

4.3 IEEE 39 Bus System

This system is widely known as the New England Test System. Figure 4.18 shows the single line diagram of the system. It consists of ten generators, each of those is equipped with

automatic voltage regulator that includes a transient gain reduction and a power system stabilizer. Complete system description can be found in [13].

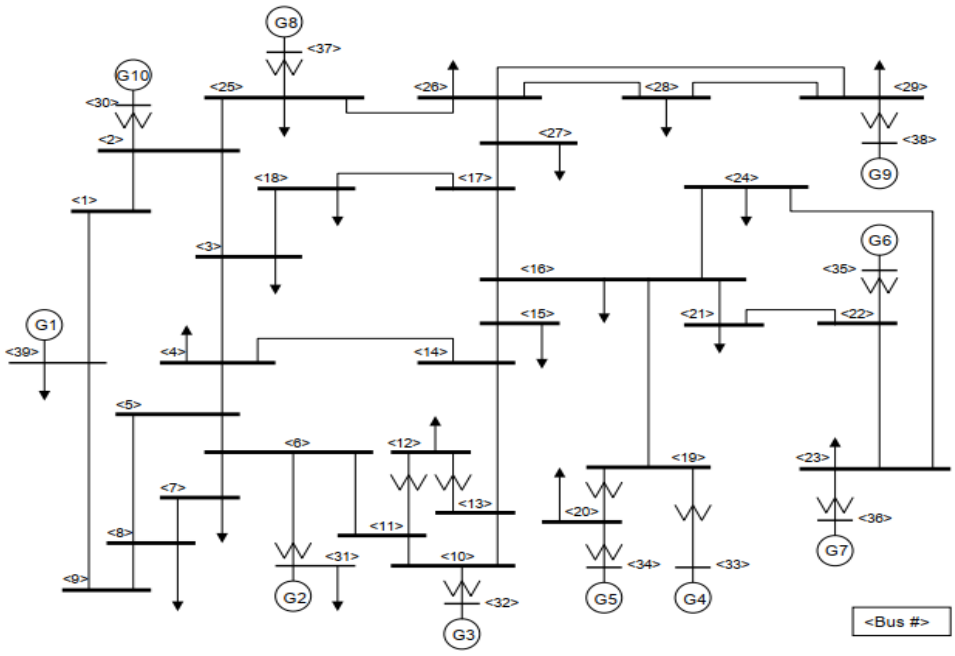

Figure 4.18 Single line diagram of the IEEE 39 bus system

4.3.1 Eigenvalue analysis

A MATLAB code was written to assess the small signal stability of the IEEE 39 bus system. The resulted eigenvalues were then compared to those obtained from the developed Simulink model. Table 4.9 presents the eigenvalues obtained from both representations.

Table 4.9 Eigenvalues Obtained from MATLAB and Simulink Models

Mode No.	MATLAB Model	Simulink Model
1	0.048±3.96i	0.204±3.84i
2	0.358±6.6i	0.308±5.7i
3	0.225±6.72	0.007±6.2i
4	0.139±6.94i	-0.0803±6.63i
5	0.1±7.25i	-0.117±7.4i
6	0.327±7.39i	-1.53±7.87i
7	-0.116±8.15i	-0.359±8.47i
8	-0.302±8.24i	-3.03±8.47i
9	-0.19±8.34i	-0.338±9.84i

Table 4.9 shows that the two representations gave slightly different eigenvalues. The reason for these differences has been discussed in section 4.1.1. Furthermore, MATLAB script resulted in a less damped modes, therefore, a design based on these modes will likely result in a favorable outcome when applied to the Simulink model.

Figures 4.19 shows the system response due to a fault on bus 14 occurring at t = 10s. The fault impedance is 0.001 PU and lasted for 6 cycles. It is seen that the system losses synchronism due to unstable electromechanical modes.

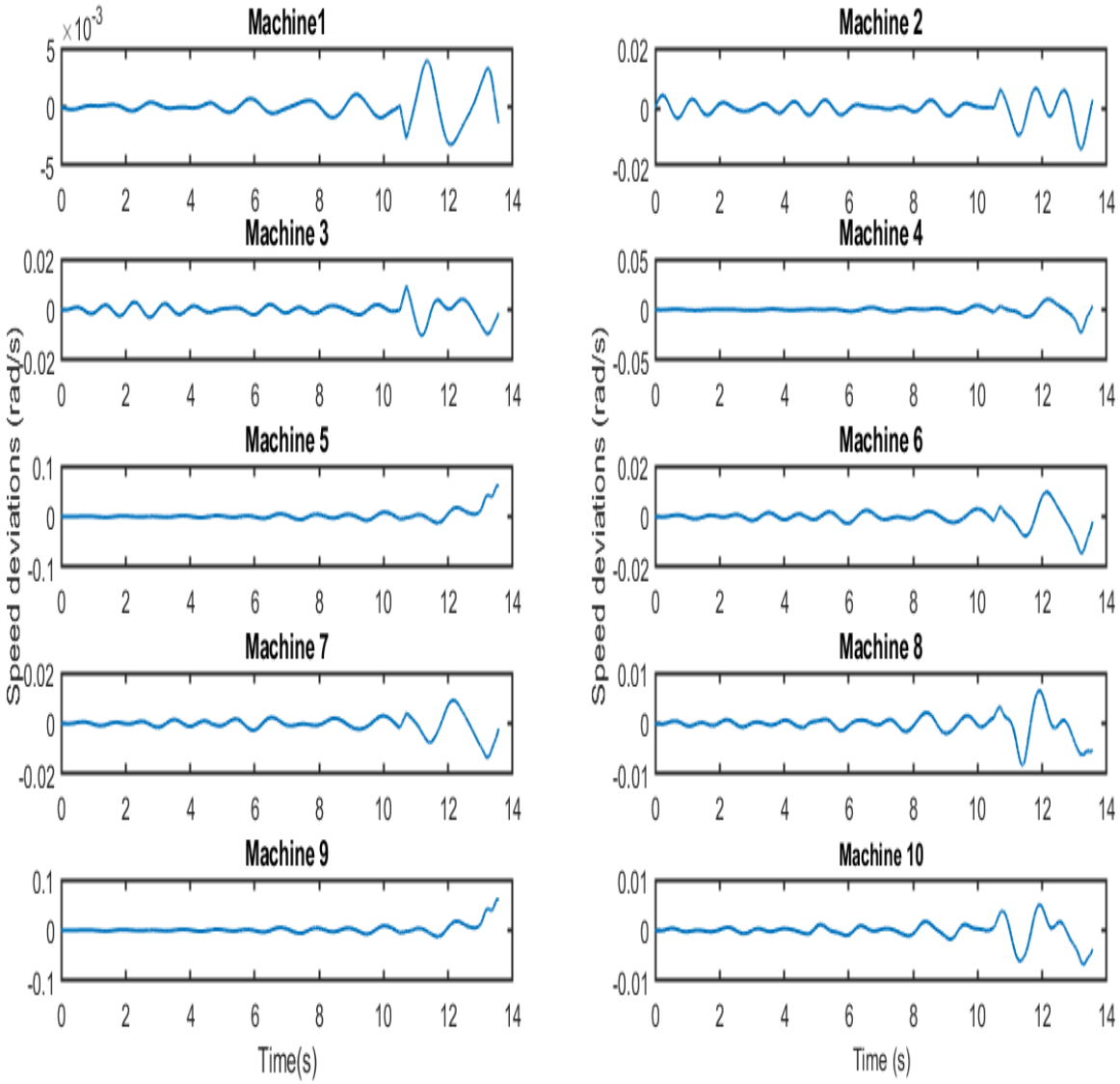

Figure 4.19 Speed deviations for IEEE 39 generators

4.3.2 Power system stabilizer tuning

Ten power system stabilizers were tuned according to the procedure in section 3.6. The only modification made is to multiply the obtained gains by factor of 10 to remedy the effect of the transient gain reduction block attached to the automatic voltage regulator (AVR). Table 4.10 shows the obtained gains and time constants.

Table 4.10 Power System Stabilizers Tuned Parameters.

Machine No.	Gain (p.u)	Time constant (s)
1	106.9	0.190
2	29.126	0.186
3	34.47	0.168
4	26.53	0.158
5	24.67	0.191
6	31.49	0.176
7	34.08	0.155
8	25.31	0.171
9	38.39	0.149
10	66.14	0.141

Figure 4.20 shows the poles of the system before and after installing the power system stabilizer. It is shown that the poles were located to the left-hand side, with minimum damping of 30%.

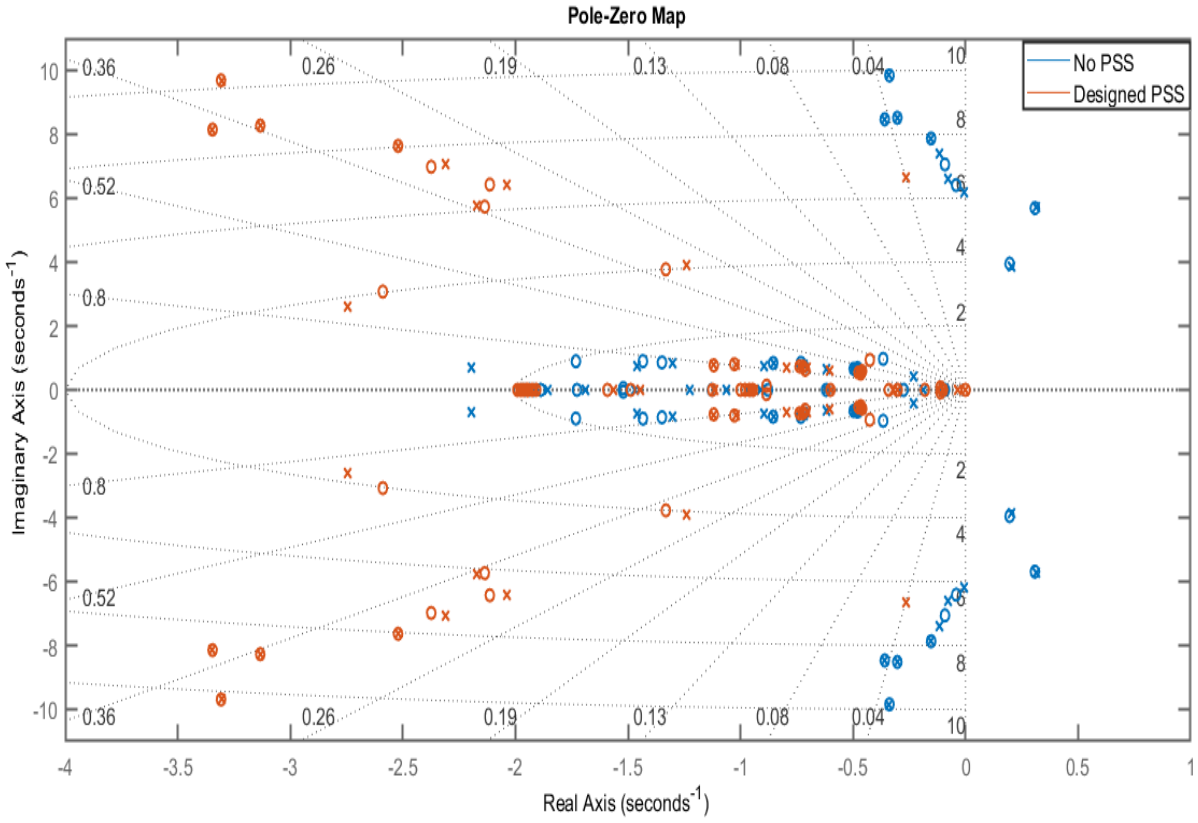

Figure 4.20 System poles before and after applying the designed PSS

4.3.3 Performance comparison

The performance of the designed PSS was compared to PSS design found on the IEEE benchmark for small signal stability [13]. Time simulation was carried out to demonstrate the effectiveness of the designed PSS. Figure 4.21 shows the system response for both stabilizer due to a fault in bus 14 while Figure 4.22 displays the pole zero map when applying both designs.

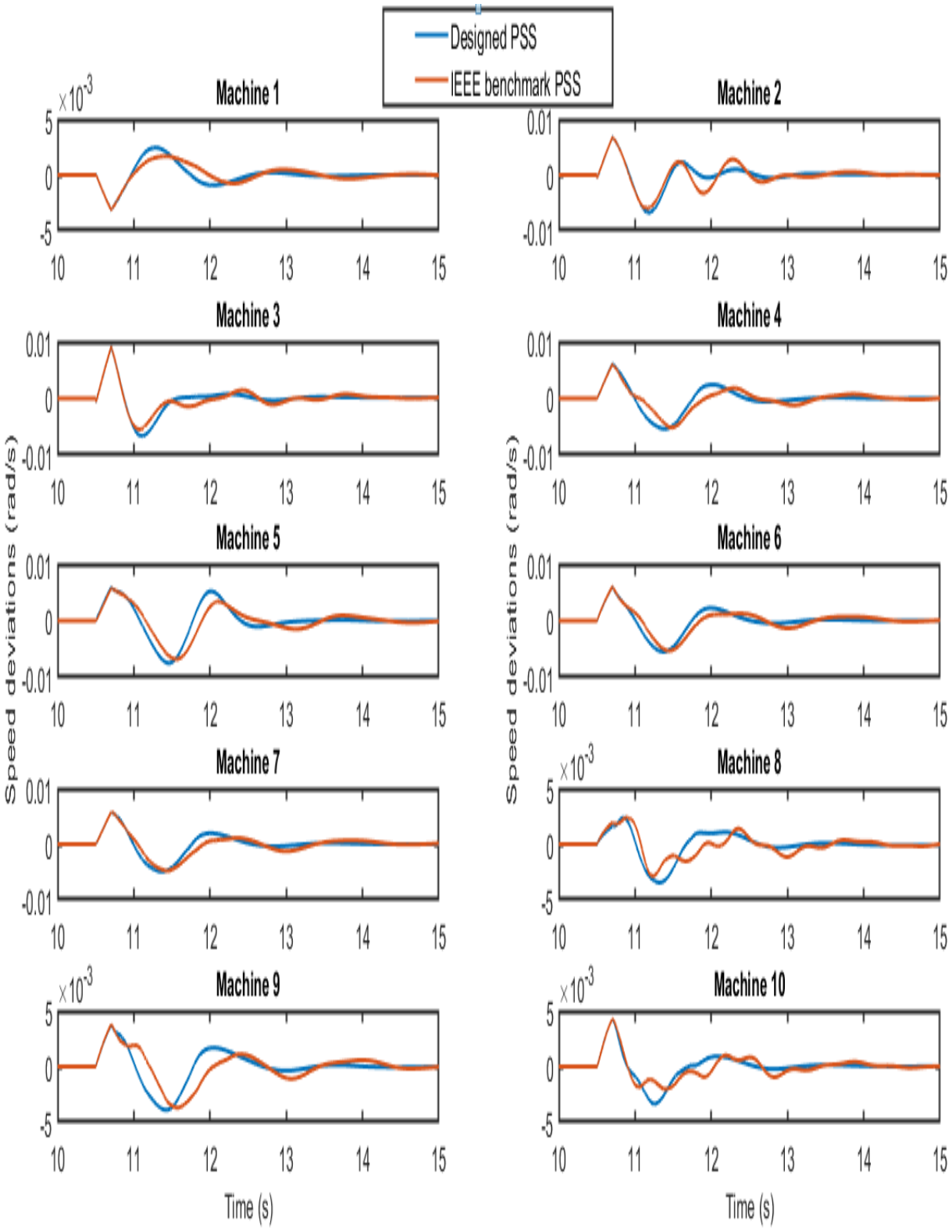

Figure 4.21 Speed deviations due to a fault on bus 14

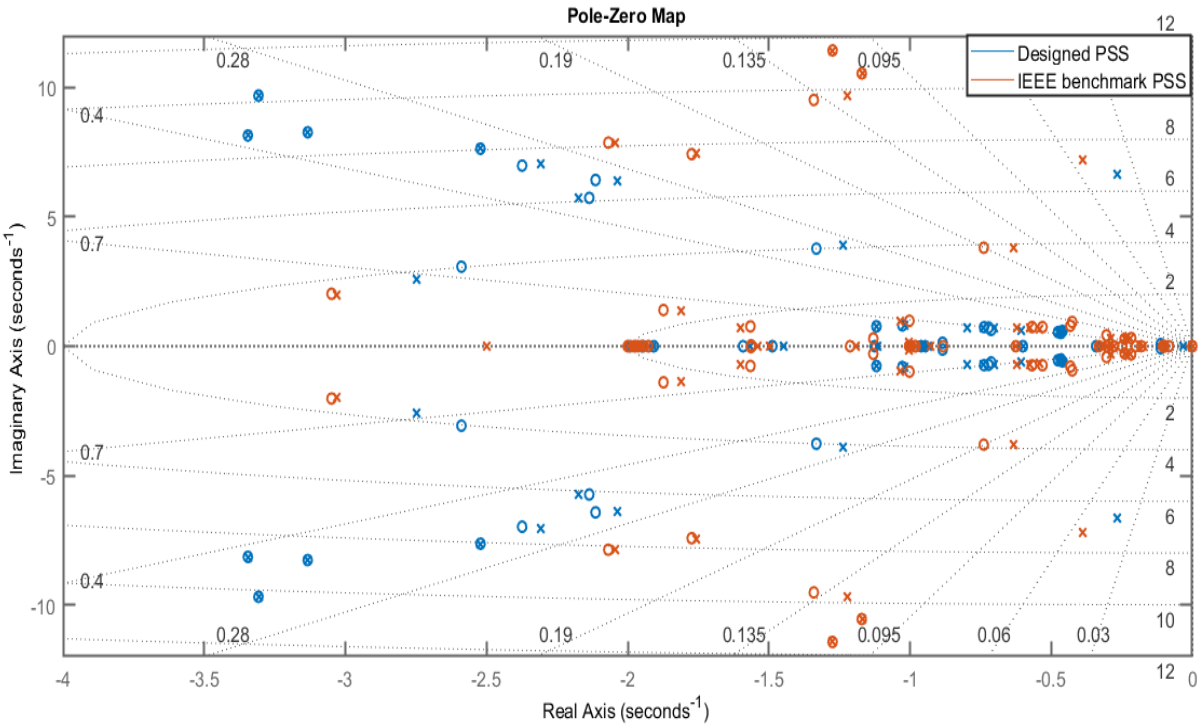

Figure 4.22 Pole zero map of both designs

Figures 4.21 and 4.22 show the superiority of the designed PSS over the IEEE benchmark PSS. In Figure 4.21, the designed PSS was able to damp the oscillations faster than design found on [13] allowing the system to recover from the fault without being stressed. Figure 4.22 shows that the new PSS provided better damping to the electromechanical modes than the PSS proposed by [13].

CHAPTER 5

CONCLUSION

This work presented a novel and simplified method to tune power system stabilizer parameters. The method analyzed the generator electrical torques and identified generators with insufficient or negative damping torques. The power system was tuned such that it provides damping torque at that poorly damped electromechanical mode.

The performance of the proposed design was examined using a variety of test systems specifically, the two areas- four-machines system, IEEE9 and IEEE 39 bus systems. The proposed PSS succeeded to provide adequate damping for the unstable/poor modes. Moreover, it was found that the simple structure proposed PSS provided better results than more complex power system stabilizers designs.

The incorporation of system admittance matrix in the methodology is what essentially makes the proposed methodology powerful when compared to other power system stabilizer designing techniques. While other methods relay on local measurement that provides little information about the reminder of the system, the incorporation of the admittance matrix provides the method with sufficient information to design a robust power system stabilizer.

It is worth mentioning that the proposed method does not require a complete small signal analysis (participation matrix calculation, right and left eigenvectors) since it only looks for the unstable/poorly damped mode frequency. This value can be obtained from simulation results.

For further validation, the suggested method was tested at different loading conditions. Although the power system stabilizer was designed at the base case loading conditions, its performance at these conditions showed high degree of adequacy and robustness.

REFERENCES

[1] D. Trudnowski, "Properties of the Dominant Inter-Area Modes in the WECC Interconnect," 2012. [Online] Available: https://www.wecc.biz/Reliability/WECCmodesPaper130113Trudnowski.pdf

[2] A. Kumar, "Power System Stabilizers Design for Multimachine Power Systems Using Local Measurements," *IEEE Transactions on Power Systems,* vol. 31, no. 3, pp. 2163-2171, 2016.

[3] G. Gurrala and I. Sen, "Power System Stabilizers Design for Interconnected Power Systems," *IEEE Transactions on Power Systems,* vol. 25, no. 2, pp. 1042-1051, 2010.

[4] P. Kundur *et al.*, "Definition and classification of power system stability IEEE/CIGRE joint task force on stability terms and definitions," *IEEE Transactions on Power Systems,* vol. 19, no. 3, pp. 1387-1401, 2004.

[5] W. G. Heffron and R. A. Phillips, "Effect of a Modern Amplidyne Voltage Regulator on Underexcited Operation of Large Turbine Generators [includes discussion]," *Transactions of the American Institute of Electrical Engineers. Part III: Power Apparatus and Systems,* vol. 71, no. 3, pp. 692-697, 1952.

[6] F. P. Demello and C. Concordia, "Concepts of Synchronous Machine Stability as Affected by Excitation Control," *IEEE Transactions on Power Apparatus and Systems,* vol. PAS-88, no. 4, pp. 316-329, 1969.

[7] M. Gibbard and D. Vowles, "Reconciliation of methods of compensation for PSSs in multimachine systems," in *IEEE Power Engineering Society General Meeting,* vol. 2, p. 1742, 2004.

[8] D. M. Lam and H. Yee, "A study of frequency responses of generator electrical torques for power system stabilizer design," *IEEE Transactions on Power Systems,* vol. 13, no. 3, pp. 1136-1142, 1998.

[9] Y. Obata, S. Takeda, and H. Suzuki, "An Efficient Eigenvalue Estimation Technique for Multimachine Power System Dynamic Stability Analysis," *IEEE Transactions on Power Apparatus and Systems,* vol. PAS-100, no. 1, pp. 259-263, 1981.

[10] E. V. Larsen and D. A. Swann, "Applying Power System Stabilizers Part II: Performance Objectives and Tuning Concepts," *IEEE Transactions on Power Apparatus and Systems,* vol. PAS-100, no. 6, pp. 3025-3033, 1981.

[11] P. Kundur, N. J. Balu, and M. G. Lauby, *Power system stability and control*. McGraw-Hill, New York, 1994.

[12] I. Kamwa, R. Grondin, and G. Trudel, "IEEE PSS2B versus PSS4B: the limits of performance of modern power system stabilizers," *IEEE Transactions on Power Systems,* vol. 20, no. 2, pp. 903-915, 2005.

[13] Benchmark Systems for Small-Signal Stability Analysis and Control, August 2015, p. 390. [Online]. Available: http://resourcecenter.ieee-pes.org/pes/product/technical-publications/PESTR18.

APPENDIX A

EXPRESSIONS FOR MATRICES $G_1(s)$ TO $G_6(s)$

$$G_1(s)=\begin{bmatrix} \frac{1}{2}\sin\left(2\delta_0 x_{dq}(s)\right)-\frac{v_{x0}\sin\delta_0 d(s)}{x_d(s)} & -\cos^2\delta_0 x_{dq}(s)-\frac{1+v_{y0}\sin\delta_0 d(s)}{x_d(s)} \\ \sin^2\delta_0 x_{dq}(s)+\frac{1+v_{x0}\cos\delta_0 d(s)}{x_d(s)} & -\frac{1}{2}\sin\left(2\delta_0 x_{dq}(s)\right)-\frac{v_{y0}\sin\delta_0 d(s)}{x_d(s)} \end{bmatrix} \quad \text{A.1}$$

$$G_2(s)=\frac{\omega_0}{s}\begin{bmatrix} \frac{v_{d0}\sin\delta_0}{x_d(s)}+\frac{v_{q0}\cos\delta_0}{x_q(s)}-i_{y0} \\ -\frac{v_{d0}\sin\delta_0}{x_d(s)}+\frac{v_{q0}\cos\delta_0}{x_q(s)}-i_{x0} \end{bmatrix} \quad \text{A.2}$$

$$G_3(s)=$$

$$\begin{bmatrix} \frac{v_{y0}-v_{x0}v_{d0}d(s)}{x_d(s)}+ & v_{q0}\sin\delta_0 x_{dp}(s)+i_{x0} & -\frac{v_{x0}-v_{y0}v_{d0}d(s)}{x_d(s)}+ & v_{q0}\cos\delta_0 x_{dp}(s)+i_{y0} \end{bmatrix} \quad \text{A.3}$$

$$G_4(s)=\frac{\omega_0}{s}\left(\frac{v_{d0}^2}{x_d(s)}+\frac{v_{q0}^2}{x_q(s)}+v_{y0}i_{x0}-v_{x0}i_{y0}\right) \quad \text{A.4}$$

$$G_5(s)=\frac{G(s).G_{avr}(s)}{x_d(s)}\begin{bmatrix} \sin\delta_0 \\ -\cos\delta_0 \end{bmatrix} \quad \text{A.5}$$

$$G_6(s)=\frac{v_{d0}G(s).G_{avr}(s)}{x_d(s)} \quad \text{A.6}$$

Where:

$$d(s)=\frac{G(s).G_{avr}(s)}{v_{t0}}$$

$$x_{dq}(s)=\frac{1}{x_q(s)}-\frac{1}{x_d(s)}$$

APPENDIX B

TWO-AREA FOUR-MACHINE SYSTEM DATA TABLES

System Data (pu on 100MVA/230KV base)

Element	From	To	Resistance (pu/km)	Inductance (pu/km)	Admittance (pu/km)	Length (km)
T-1	1	5	0.0	0.0167	0.0	-
T-2	6	2	0.0	0.0167	0.0	-
T-3	11	3	0.0	0.0167	0.0	-
T-4	10	4	0.0	0.0167	0.0	-
Line-1	5	6	0.0001	0.001	0.00175	25
Line-2	6	7	0.0001	0.001	0.00175	10
Line-3	7	8	0.0001	0.001	0.00175	110
Line-4	8	9	0.0001	0.001	0.00175	110
Line-5	9	10	0.0001	0.001	0.00175	10
Line-6	10	11	0.0001	0.001	0.00175	25

Generators Data (pu on 900MVA/20KV base)

	Generators Data					Exciters Data	
	X_q	X_d	X'_d	H	T_{d0}	K_e	T_e
Gen.1	1.7	1.8	0.3	6.5	8	200	0.001
Gen.2	1.7	1.8	0.3	6.5	8	200	0.001
Gen.3	1.7	1.8	0.3	6.175	8	200	0.001
Gen.4	1.7	1.8	0.3	6.175	8	200	0.001

System Total Generation

	Active Power (MW)	Reactive Power(MVAR)	Terminal Voltage (pu)
Gen.1	700	91	$1.05<10.22^0$
Gen.2	700	117	$1<0^0$
Gen.3	719	82	$1.05<-15.\ 8^0$
Gen.4	700	82	$1.05<-26.03^0$

System Loads

	Active Power (MW)	Reactive Power(MVAR)	Shunt Capacitors Reactive Power (MVAR)
Load.7	967	-87	200
Load.9	1767	-87	350

APPENDIX C

IEEE9-BUS SYSTEM DATA TABLES

System Data (pu)

Element	From	To	Resistance (pu)	Inductance (pu)	Admittance (pu)
T-1	1	7	0.0	0.0625	0.0
T-2	2	9	0.0	0.0586	0.0
T-3	3	4	0.0	0.0576	0.0
Line-1	4	5	0.01	0.085	0.176
Line-2	4	6	0.017	0.092	0.158
Line-3	5	7	0.032	0.161	0.306
Line-4	6	9	0.039	0.17	0.358
Line-5	7	8	0.0085	0.072	0.149
Line-6	8	9	0.0119	0.1008	0.209

Generators Data (pu)

	Generators Data					Exciters Data	
	X_q	X_d	X'_d	H	T_{d0}	K_e	T_e
Gen.1	0.8645	0.8958	0.1198	6.4	5.9	200	0.05
Gen.2	1.2578	1.3125	0.1813	3.01	5.89	200	0.05
Gen.3	0.0908	0.1455	0.0608	23.64	8.96	200	0.05

System Generation

	Active Power (MW)	Reactive Power(MVAR)	Terminal Voltage
Gen.1	163	67	$1.025<9.3^0$
Gen.2	85	-109	$1.025<4.7^0$
Gen.3	72	27	$1.04<0^0$

System Loads

	Active Power (MW)	Reactive Power(MVAR)
Load.5	125	50
Load.6	90	30
Load.8	100	35

VITA

Akram Saad was born in Omdurman, Khartoum, Sudan to his parents Amir and Najwa. He is the fourth of six children. Mr. Saad received his Bachelor of Science degree in electrical and electronics engineering - power system concentration- in 2014 from the University of Khartoum in Khartoum, Sudan. After graduation, Mr. Saad worked as a part-time teaching assistant at the Department of Electrical and Electronic Engineering at the University of Khartoum for two semesters, after which he joined the CTC Group's graduate development program, where he spent a year under training. In August 2016, Mr. Saad accepted a graduate assistantship at the University of Tennessee at Chattanooga to pursue his master's degree in Electrical Engineering, and will graduate in August 2018. Mr. Saad is currently interning at Patterson Power Engineers, LLC as a protection engineer.